Earth’s Rotational (Spin) Axis

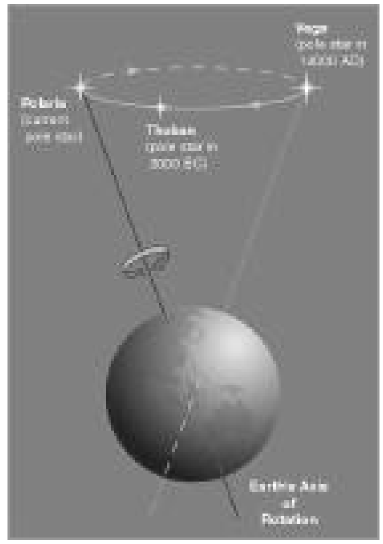

Introduction to Earth Rotation

- Earth does not rotate at a constant speed, instead

✓ the rotation rate is variable, i.e. the length of day is changing

✓ the rotation axis moves with respect to geography (i.e. Polar Motion; quasi-stationary seen from inertial space)

- Reasons:

  a) Torques exerted by sun, moon, planets (Precession, Nutation)

  b) Rotational axis & Figure axis not aligned (Wobble)

  c) Tides & Geodynamic Processes on & within the Earth

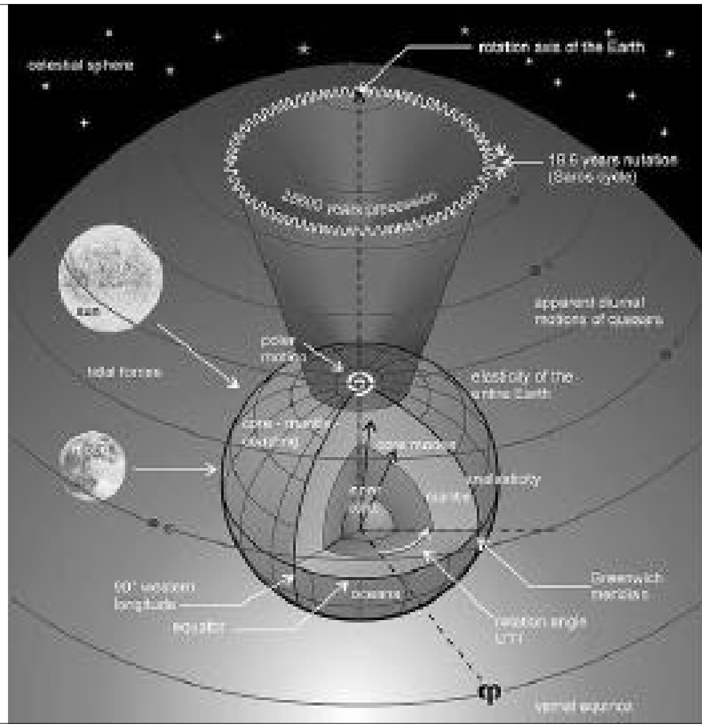

Modern Geodetic Techniques for Earth Rotation Measurement

- Very Long Baseline Interferometry (VLBI)
- Satellites of the Global Positioning System (GPS) or of the Global Navigation Satellite System (GLONASS)
- Laser Ranging to artificial earth satellites of the Lageos- or Starlette (Satellite LAser Ranging)
- Earth remote sensing satellites like ERS1, ERS2 and TOPEX/POSEIDON
- Laser Ranging to the retroreflectors deployed on the Moon’s surface (Lunar Laser Ranging)

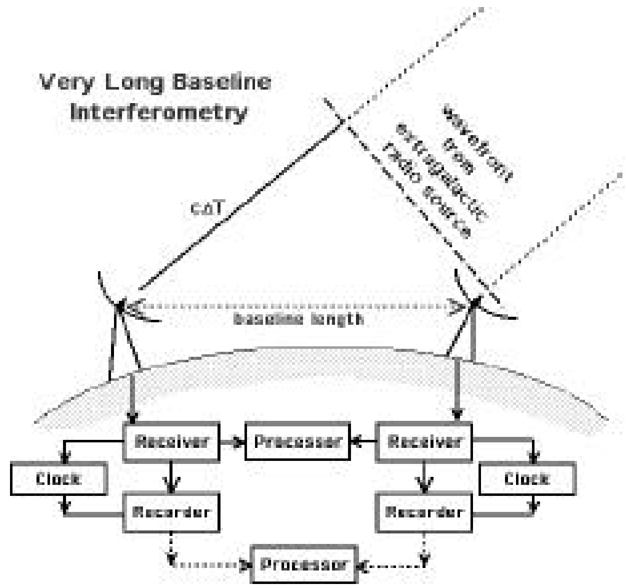

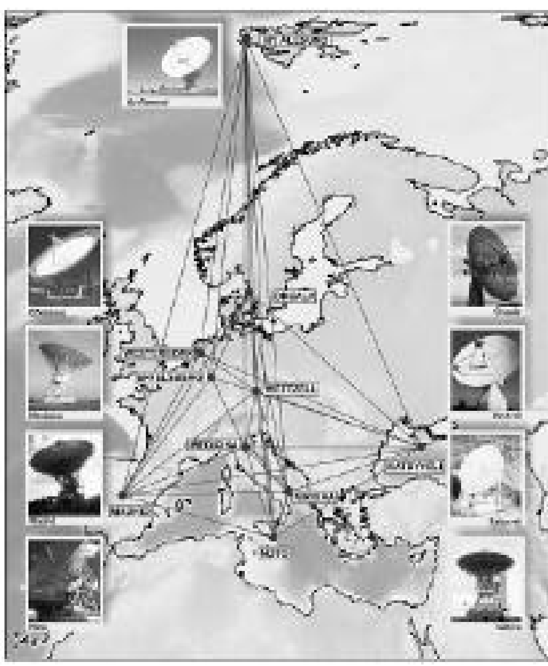

The
European
Geodetic
VLBI
Network

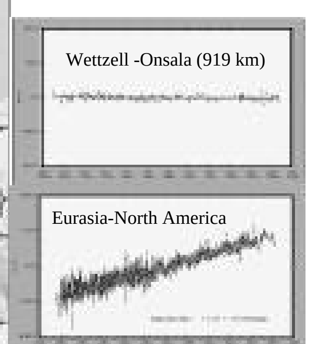

Very Long Baseline Interferometry

Employing state-of-the-artgeophysical models and a sophisticated least squares parameter estimation process the delays are adjusted and the relevant parameters like *station coordinates, baseline lengths, radio source positions* and Earth rotation parameters (*precession, nutation, polar motion and Universal Time*) are determined.

Lunar Laser Ranging (LLR)

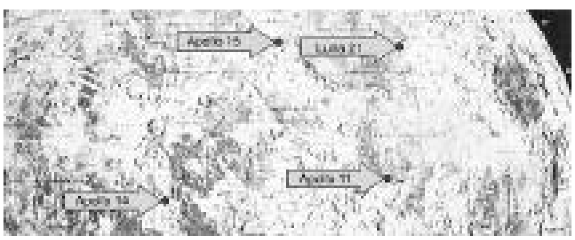

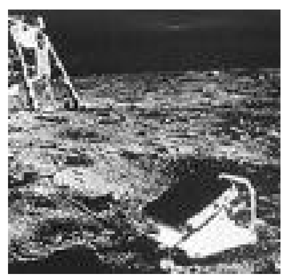

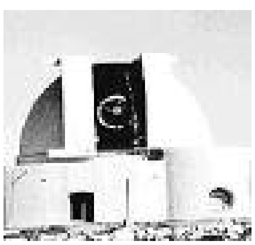

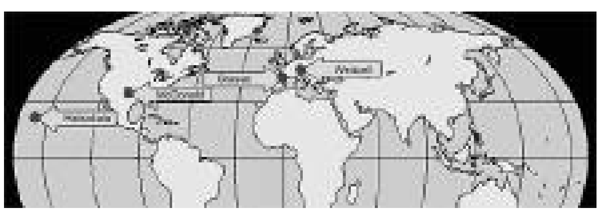

Lunar Laser Ranging (LLR)

- The Earth-Moon distance varies between 56 and 64 Earth radii.
- The observatories fix a reference frame on Earth & the reflector arrays on the Moon.
- By analyzing the observations (round trip travel times of laser pulses), one can determine the Earth Rotation, parameters describing the dynamics of the Earth-Moon system and relativistic quantities.

Satellite LAser Ranging

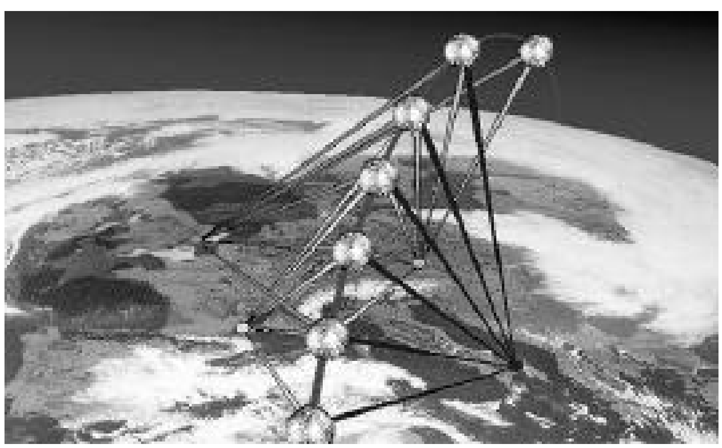

High orbiting satellites (LAGEOS I and II, 6000 km; ETALON, GPS 20000 km) are in particular suitable for the estimation of the EOP.

Satellite LAser Ranging (SLAR)

- The satellite's state at any time is the set of its position and velocity as well as parameters which appear in the dynamic acceleration model or the measurement model. The motion of the satellite is governed by a differential equation system that is integrated to determine the state at any later time. Errors in initial values and models necessitate the introduction of observations to the real satellite's motion to obtain a better trajectory.
- Observation equations taking the partial derivatives and the difference of calculated and observed distance from the orbit determination can be solved for the parameters of interest.
- For EOP, a global network of SLR stations renders the estimation of the point about which the stations are rotating during the observation time. A transformation to an earth-fixed reference frame yields the pole coordinates.

Terminology

- Length of Day (LOD)
- Precession, Nutation
- Polar Motion, True Polar Wander, Wobble
- Chandler Wobble, Annual Wobble
- Near Diurnal Free Wobble
- Tidal Friction & Nontidal Acceleration
- Pole Tides
- Decade Fluctuations
- Tisserand System & Conventional Terrestrial System

Variable Rotation Rate (1)
(change in "the length of day")

- 50 years ago, time was kept by watching transit time of stars. This is Universal Time (UT) or Greenwich time
- When atomic clocks were developed in 1950's, it was found that UT didn't agree with atomic clock time (AT). Since AT is "constant", UT is variable. For an increase in rotation rate, there is a decrease in the length of day (***LOD***):

$$\frac{\Delta LOD}{LOD_o} = -\frac{\delta\Omega(t)}{\Omega_o}$$

and $\frac{2\pi}{\Omega_o} = LOD_o$ = number of seconds per day if there were no variation in rotation. The change is of the order of 10^{-8}

Variation in LOD

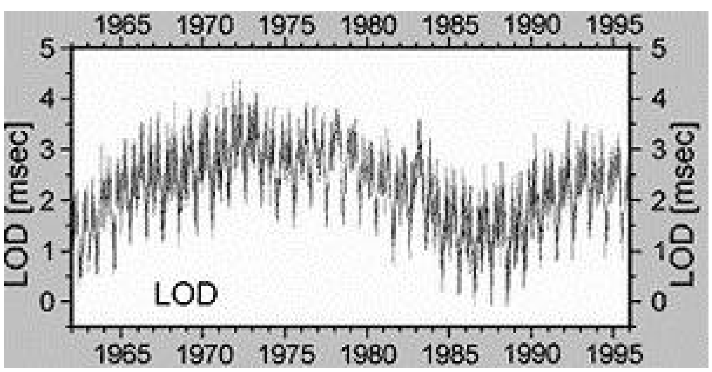

These variations consist mainly of a secular trend, long-period variations and seasonal variations with an annual and a semiannual period.

Decade Fluctuations of LOD

- Decade fluctuations in LOD are believed to be due to the transfer of angular momentum between the fluid core and the solid mantle. This requires torque at the Core Mantle Boundary (CMB)
- Possible Mechanisms:

✓ Pressure or inertial coupling due to the ellipticity of the CMB

✓ Topographic Coupling

✓ Viscous coupling

✓ Electromagnetic Coupling

LOD variation revealed from Historic Eclipse Observations

Historical eclipse observations

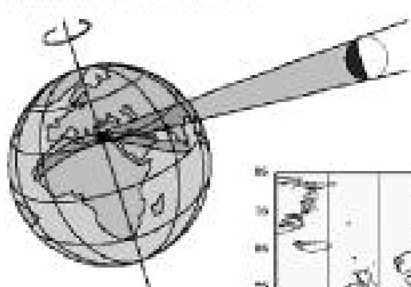

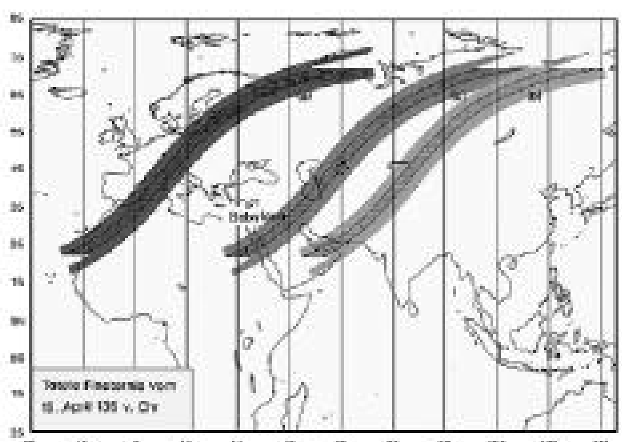

The shadow path of an ancient Babylonian solar eclipse computed with several assumptions:
a) a constant angular Earth's rotation rate.
b) a constant change in the Earth's rotation rate due only to tidal friction.
c) In accordance with the observed Eclipse circumstances.

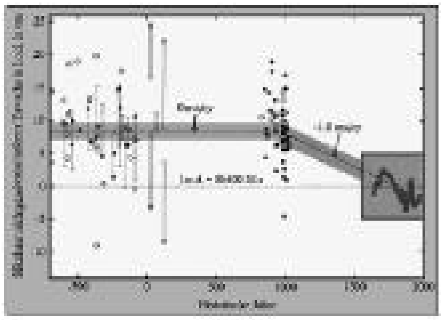

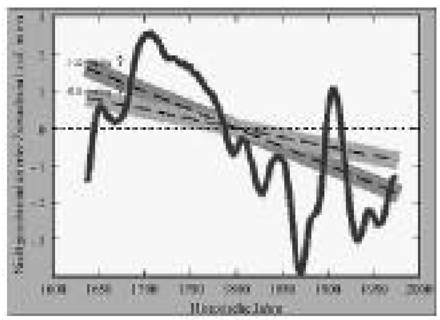

LOD Variations

Non-tidal changes of the Earth's rotation rate as observed from telescopic data. Accurate astrometrical satellite data exists only for the last 25 years. Secular changes of the Earth's rate of rotation can only be determined with the help of medieval and ancient astronomical observations.

According to Stephenson & Morrison a long-term fluctuation in the l.o.d. with a semi-amplitude of some 4 ms and a period of 1500 yr may exist.

A careful critical review of medieval Arab eclipse records shows that the historical sources are not in contradiction with a constant secular change in the Earth's rotation rate.

Coral & Stromatolite data shows that 500 Ma BP,

there were ~420 days/year (due to tidal deceleration)

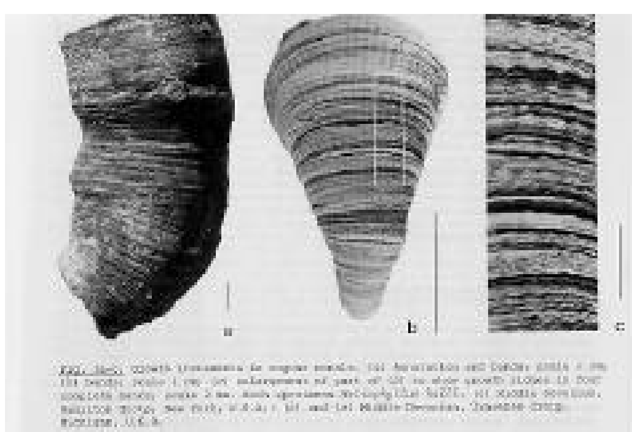

Variable Rotation /Spin Rate (2)

- Paleo-rotation data: there were ~420 days/year during Cambrian period ~500 Ma ago(Tidal Friction)
- Linear increase of ~2 ms per century (Tidal Friction & Postglacial Rebound)
- Decade fluctuations of about 4-5 ms over 20-30 years
- Annual and shorter period fluctuation (atmosphere)
- Modern techniques: VLBI (very-long-baseline Interferometry), LLR (lunar laser ranging) & SLR (satellite laser ranging). Accuracy: better than 0.1 ms for averages over 3-5 days. (Results improve when longer averaging times are used.)

Reference Frame for Deformable Earth

- Tisserand System -requires the residual motions of all parts of the Earth to be a minimum in this so called. This reference frame can be thought of as being realised by the rotation of a rigid body.
- Conventional Terrestrial System (CTS) is a rigid reference frame co-rotating with the Earth in inertial space with angular velocity Ω

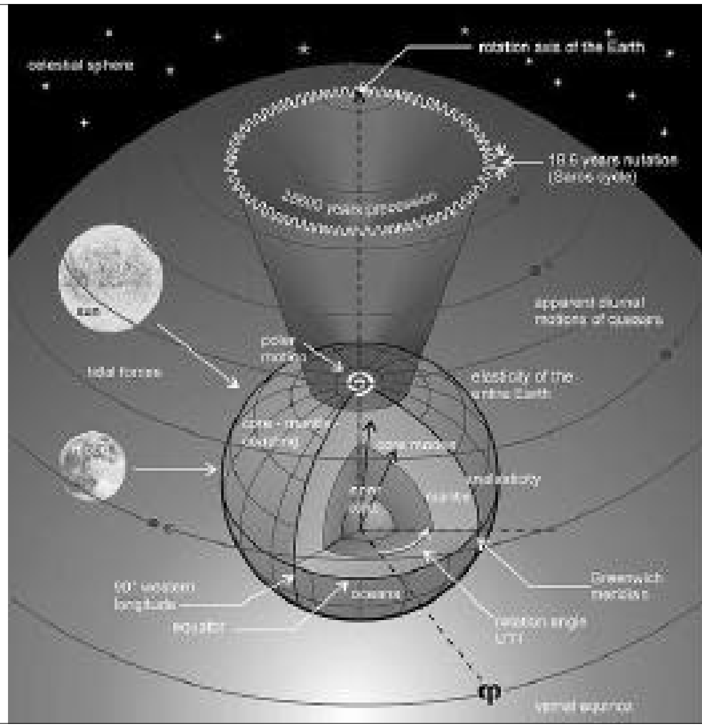

Nutation & Precession

- These are motion of the spin (CTS) axis *with respect to inertial space* (in practice, relative to a quasi-inertial frame tied to the ecliptic and equinox at a certain epoch).
- Precession generally refers to the slow motion with period of ~26,000 years while Nutation superposes a small nodding motion with a period of 18.6 years and an amplitude of 9.2 seconds of arc.
- They are caused by the gravitational torques of the Moon and Sun on the spinning Earth's equatorial bulge. (The plane of the Moon's orbit around the Earth is tilted by about 5^{o} from the plane of the Earth's orbit around the Sun.)

Nutation in Longitude detected by VLBI

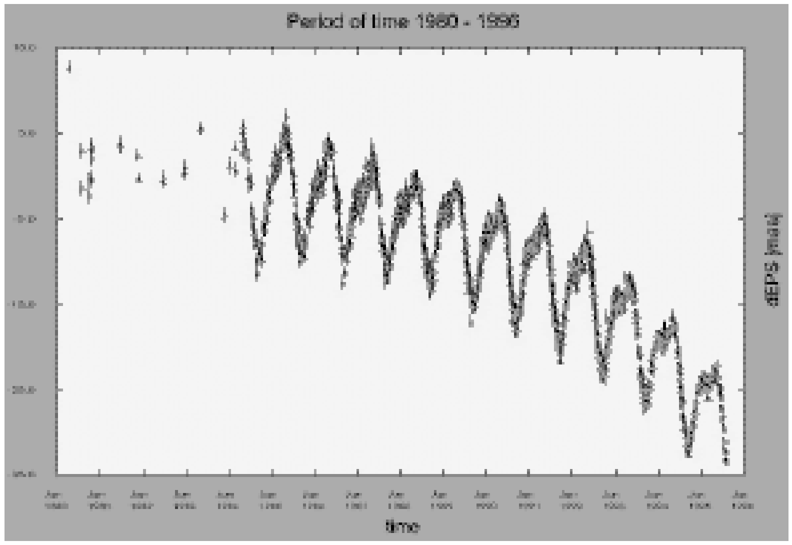

Nutation as seen by VLBI

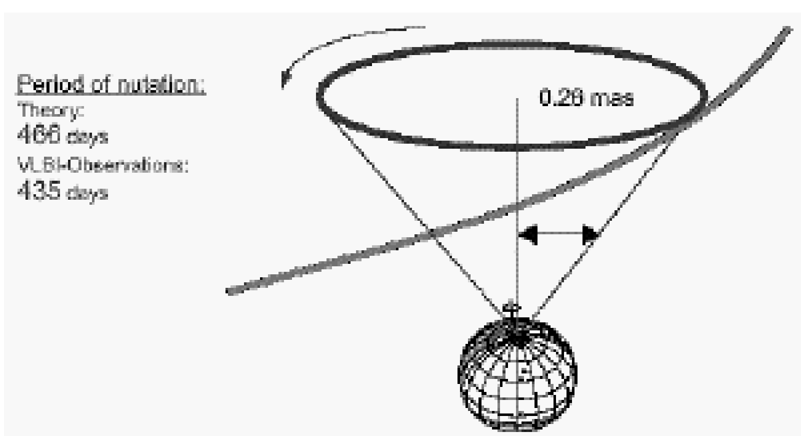

Polar Motion measured by VLBI

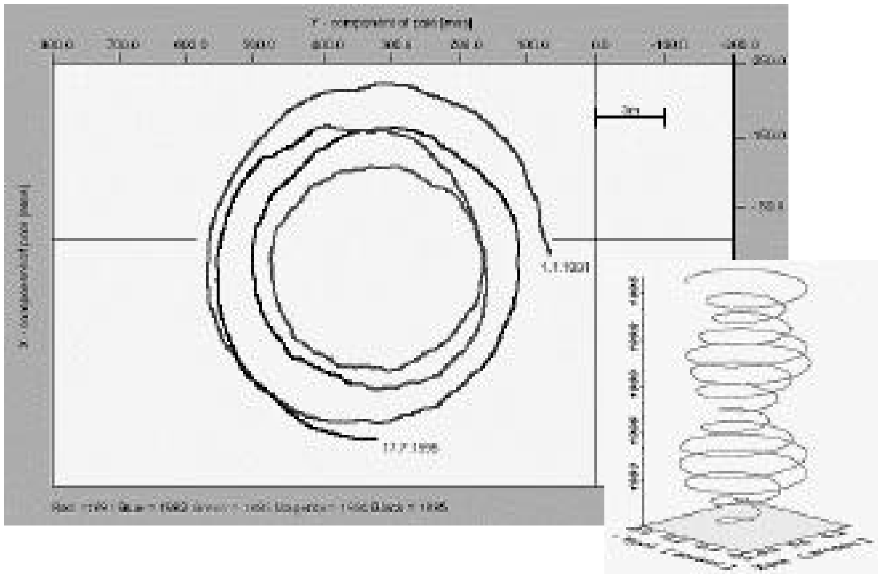

Polar Motion- wobble & polar wander

- Polar Motion - motion of the spin (CTS) axis *with respect to the earth's surface*. Although the departure of Ω from e_3 is under 0.4", it varies in both space and time. Wobble is the periodic polar motion while Polar Wander is the aperiodic drift superposed. For an observer at the Earth's surface, Polar Motion results in latitude variations and variation in LOD.
- Polar motion is generally due to deformation *within* the Earth (wind, ocean current, mantle and core flow) and the excitation has periods much longer than one day as seen by an observer on the Earth.
- Motion which has long period as seen from Earth is actually diurnal prograde motion that is seen from inertial space. Motion which is approximately diurnal as seen from the Earth has long period as seen from inertial space. So, for the wobble motion, the earth fixed axis moves around diurnally in inertial space.

Polar Motion (continue)

- In fact, nutation cannot occur without some accompanying polar motion or vice versa. For example, a small part of polar motion is the ‘dynamical variation of latitude’ as Ω traces out a nearly diurnal retrograde circuit in the CTS of amplitude ~0.02", due to the forced nutations.
- Free Chandler wobble (period ~ 433 sidereal days) and forced Annual wobble (amplitude ~0.1 arcsec or 5 m)
- Polar wander rate of ~1°/Ma towards Hudson Bay today (due to postglacial rebound)
- Longer term True Polar Wander & Continental Drift

ILS data showing Secular (True) Polar Wander (blue lines) superposed on the oscillatory signal.
The 7 year beat in the signal is a consequence of the superposition of The 12 month forced annual wobble and the 14 month Chandler wobble.

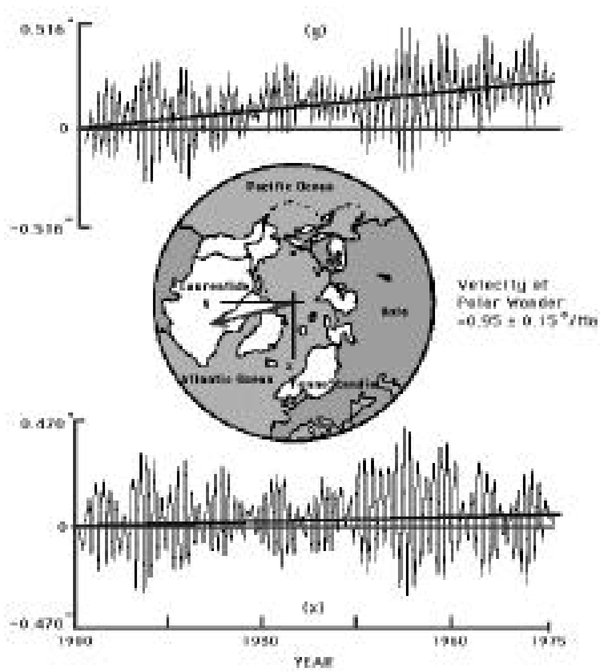

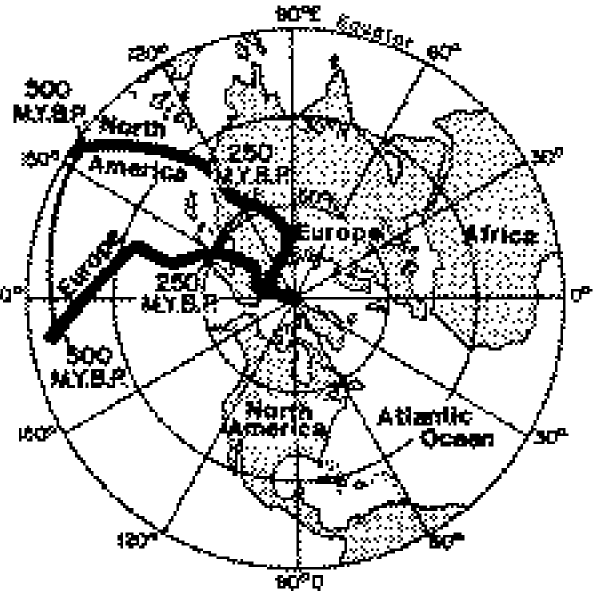

FIGURE 16 Polar-migration curves for North America and Europe. To overlay these two curves we would have to move North America eastward, which would close the Atlantic Ocean and by uniting North America and Europe form the ancient continent of Pangaea. [Figure from Keith Runcorn.]

3-D Simulations of Mantle Convection and the Earth's True Polar Wander

Paul Tackley, David Stevenson, Gary Glatzmaier

True Polar Wander (TPW) in a mantle convection simulation at Ra= 1.5x 10^6. Time variation of the difference between largest and second largest principal moments of inertia (right); Time variation of the ratio of TPW velocity to average (r.m.s.) convective velocity (bottom); path of rotationpole relative to mantle reference frame during simulation (bottom right).

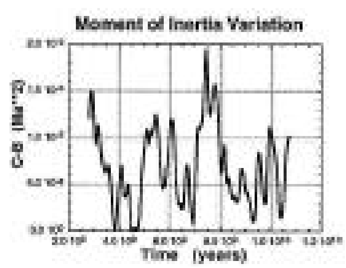

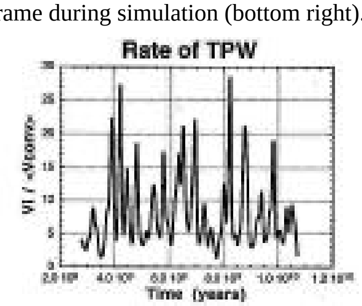

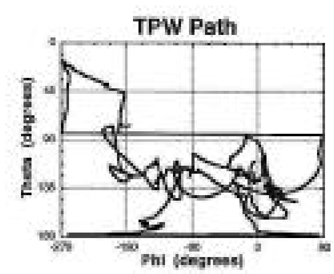

Chandler Wobble

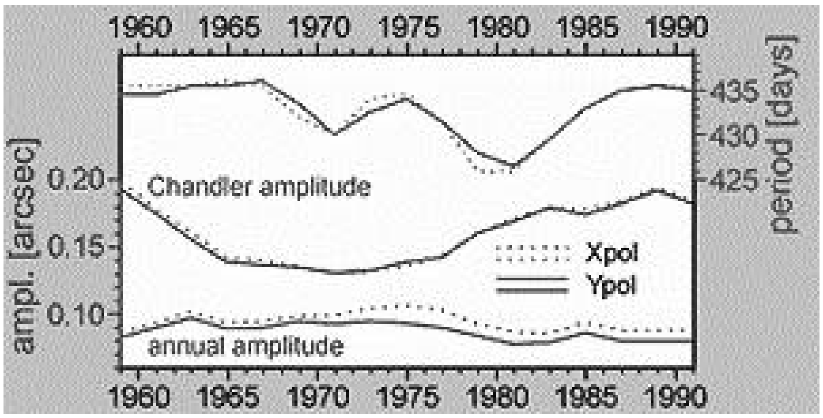

Chandler Wobble (1)

- Discovered in 1891 by S. C. Chandler. This motion, due to the dynamic flattening of the Earth, appears when the rotation axis does not coincide with one of the main axes of inertia. Without any external torque, the total angular momentum remains constant in magnitude and direction, but the Earth spins so that related to its surface, the instantaneous rotation axis moves around the main inertia axis.
- The observed period of Chandler wobble is about 433 sidereal days. (In inertial space, this motion is a quasi-diurnal mode of which the period equals 1+(1/433) day.) Some studies found several (2-5) peaks in the Chandler band. The observed amplitudes about 0.1-0.2 arcsec.

Chandler Wobble (2)

- For a rigid Earth, Euler showed that the pole displacement in the terrestrial frame produces a latitude variation with a period of 305 days.
- If one takes into account of the elasticity of the Earth, then the period increases to 445 days.
- Including the fluid core below the elastic mantle would reduce the period to about 405 days.
- Further inclusion of the small pole tide set up in the oceans by centrifugal force would increase the period by ~30 days
- If one accounts for dissipation in the mantle, core and oceans, then the predicted period would come close to the observed period of about 433 days.

Chandler Wobble (3)

- Chao (1983) explains the multiple peak structure in the Chandler band with the existence of non-elastic layers in the Earth (e.g. hydrosphere, asthenosphere & outer core) and their coupling with the visco-elastic spheres of the Earth
- The broadening of the Chandler frequency give quality factor Q~179 (i.e. decay time ~68 years), so that the amplitude would quickly dampen to zero unless some mechanism or combination of mechanisms are exciting it
- Plag (1997) hypothesized that the Chandler wobble is a forced, quasi-periodic motion close to a resonance period

Chandler Wobble (4)

- This free oscillation can be excited by mass redistribution in atmosphere, oceans and mantle (due to earthquakes).
- However, the changes in moment of inertia due to earthquakes are orders of magnitude too low and the occurrence of earthquakes are not frequent enough to sustain Chandler wobble. In the 1990's, attention turned to atmospheric forcing as the main cause of Chandler wobble
- Gross (2000) reports that the principal cause of the Chandler wobble is fluctuating pressure on the bottom of the ocean, caused by temperature and salinity changes and wind-driven changes in the circulation of the oceans. Gross calculated that two-thirds of the Chandler wobble is caused by ocean-bottom pressure changes and the remaining one-third by fluctuations in atmospheric pressure. Apparently, the effect of atmospheric winds and ocean currents on the wobble was minor

Correlation of Annual Wobble (y-component) & LOD with Atmospheric Angular Momentum

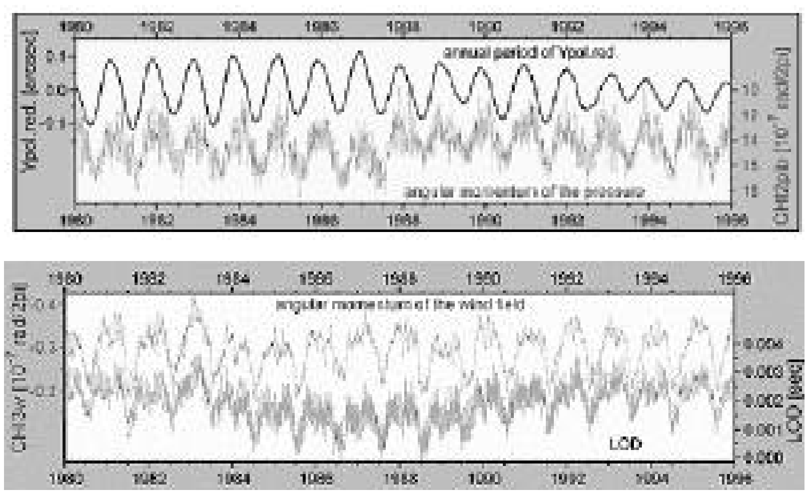

CMB Ellipticity & Free Core Nutation (Near Diurnal Free Wobble)

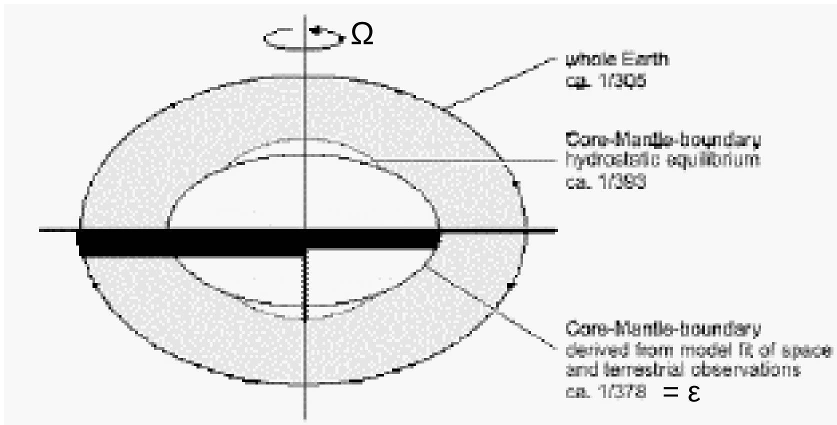

$$\sigma_{NDFW} = -\left(1 + \varepsilon \frac{C}{C_m}\right)\Omega \qquad \sigma_{NDFW} = \sigma_{FCN} - \Omega$$

Near Diurnal Free Wobble (NDFW) & Free Core Nutation (FCN)

- The CMB is elliptical, then the inertia of the core would resist the tilt of the mantle by inertial coupling. Thus, if the rotation axis of the mantle and core become misaligned, then the restoring forces at the elliptical CMB will try to realign the two axis. Because the earth is a fast spinning gyro, the reaction is a damped wobble of the instantaneous rotation axis around the figure axis (NDFW) when observed in the terrestrial reference frame. The moton of the pole is retrograde about the body axis with period ~ 1 sidereal day (differ by about 4 minutes).
- Viewed from the celestial frame (e.g. VLBI) it is called Free Core Nutation (FCN) and has a period of 432 days.

Near Diurnal Free Wobble (NDFW) & Free Core Nutation (FCN)

- The closeness of the frequencies of the NDFW mode and the diurnal tidal frequency band means that there is resonance between them. The NDFW resonantly amplifies nearly diurnal tides and annual and semiannual nutations.
- Observing the NDFW / FCN is thus very useful to measure the CMB flattening and to obtain information about the dissipation effect at this interface.
- Existence of the solid inner core leads to 2 additional eigenmodes, an inner core wobble with frequency far outside the diurnal band and a prograde free inner core nutation with its associated wobble.

Superconducting Gravimeter Observation of NDFW-FCN at Postdam

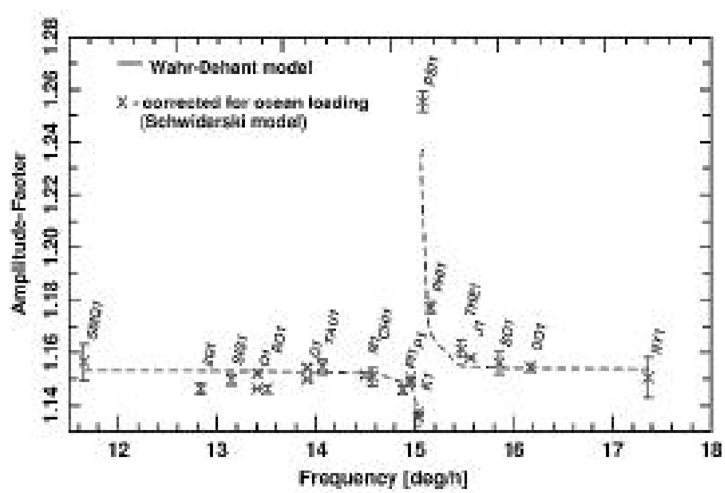

Near Diurnal Free Wobble (NDFW) & Free Core Nutation (FCN)

- Existence of the solid inner core leads to 2 additional eigenmodes, an inner core wobble with frequency far outside the diurnal band and a prograde free inner core nutation with its associated wobble.
- Unambiguous direct observation of the FCN with an amplitude of 174 μas was achieved by Herring & Dong (1994) in an analysis of 8 years of VLBI data. The wobble amplitude is 400 times smaller and is thus more difficult to measure
- Jiang & Smylie (1995) also claimed the detection of a retrograde nutation with a period of 43120 solar days in the nutation data obtained with VLBI.

Earth Tides

- Body Tides
- Ocean Tides

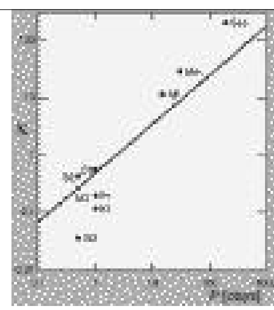

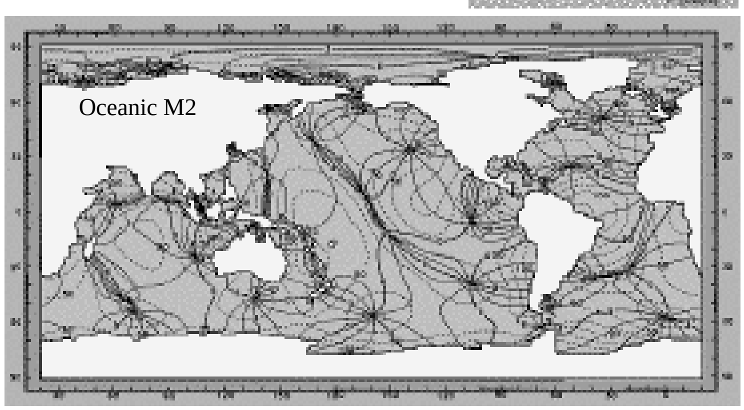

Influence of ocean tides on polar motion

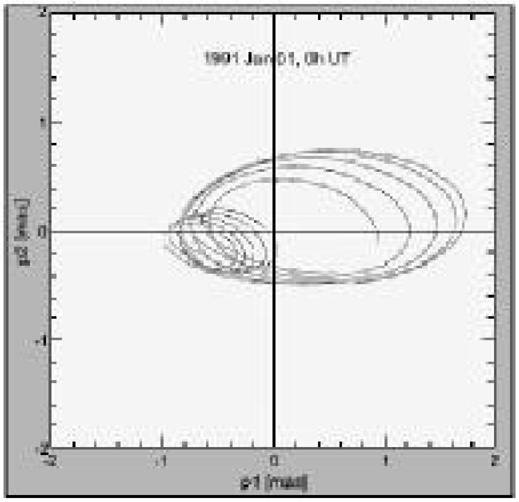

Polar motion due to the superposition of the influences of 6 partial tides in the semidiurnal (M_2, S_2 , N_2) and diurnal (K_1, O_1 , P_1) tidal bands.

Although the sectorial excitation due to the M_2-tide has no direct influence on polar motion because of its symmetry, the existence of a M_2 -part with tesseral distribution of amplitudes in the unsymmetric world oceans can be observed. This excites an indirect influence of about 0.5 mas in polar motion.

Influence of ocean tides on UT1

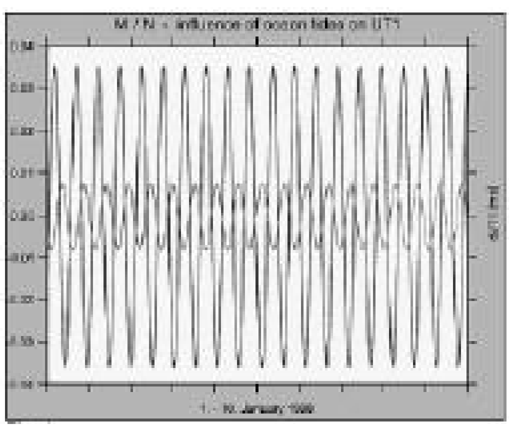

This shows the influence on UT1 due to the M_2 - and N_2 -tide for 10 days.

Variations in UT1 can be computed using the component of the total oceanic angular momentum parallel to the Earth's axis of rotation. Introducing angular momentum values from an ocean tidal model the amplitudes and phases for the influence of special partial tides on UT1 can be determined.

Pole Tide (1)

- Tide gauge data shows that in North Sea and Baltic Sea, there is a statistically significant signal at Chandler Wobble frequency, with amplitude of a few cm - i.e. several times larger than expected from the equilibrium theory
- The pole tide is not due to astronomical forcing, as are the luni-solar tides
- Poles Tides are due to changes in the centrifugal forces during Chandler wobble which produce a signal in sea level at the same frequency

Pole Tide (2)

- Whether the response of sea level to the Chandler wobble (the Pole Tide) is equilibrium or dynamic will determine if the oceans can be a substantial sink of the energy of the wobble, and, therefore, will possibly constrain an alternative mechanism, namely mantle anelasticity at low frequencies. Since Pole tides are not due to astronomical forcing, there is no a priori reason for expecting an equilibrium response
- Recent models found that without the need of a non-equilibrium oceanic pole tide, the sea level variability at the Chandler Wobble frequency can be explained for the North Sea in terms of meteorology alone. It is unknown, however, whether the wind-stress signal is connected to the wobble of the axis of rotation of the Earth, either as a product of the wobble or as an excitation mechanism of the wobble. These questions remain the subject of further research

Tidal Friction (1)

- The Moon deforms the Earth and oceans into the ellipsoidal shape
- The orientation of the ellipsoidal bulge is fixed with respect to the Moon, while the Earth rotates at 1 cycle/day relative to the bulge. The resulting lunar tides are time dependent, with frequencies equal to integral multiples of 1 cycle/day, modulated by the frequencies of the lunar orbit (e.g. 1 cycle per 27.7 days and 1 cycle per 13.7 days)

Tidal Friction & Earth-Moon Distance

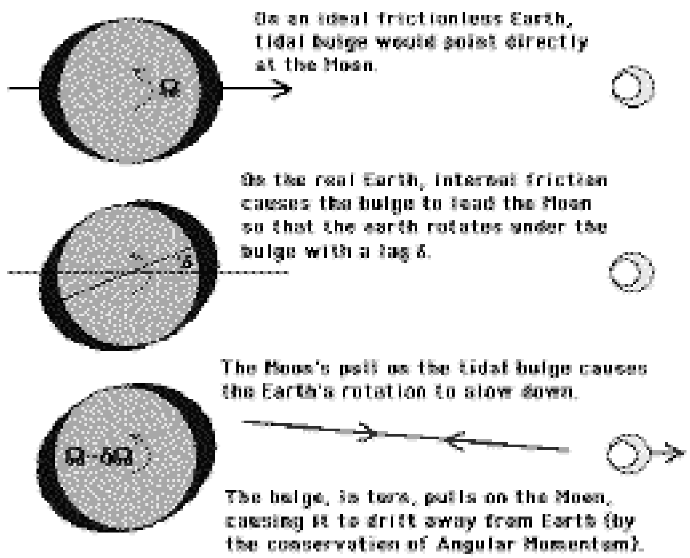

Tidal Friction (2)

- If there were no energy dissipation in the Earth and oceans, the ellipsoidal bulge should point towards the Moon. However, there is some dissipation and the maximum tidal uplift occurs shortly after the Moon is overhead, and the bulge leads the Earth-Moon vector by a small angle δ 3. (From δ, seismic attenuation or quality factor Q can been estimated to be ~20 and is lower than most seismic estimates.)
- The Moon's gravitational force acts on the tide bulge to produce a clockwise torque on the Earth, opposite to its rotation.Thus, there is an increase in LOD (Tidal Deceleration) of ~ 2.3 ms/century
- There is a similar, although smaller, effect from the sun

Tidal Friction (3)

- Most of the tidal energy dissipation is believed to occur in the oceans. It is still not entirely clear whether most of the dissipation occurs in shallow seas or in deep oceans
- The Earth's tidal bulge causes a counter-clockwise torque in the direction of the Moon's motion, thus increasing its angular momentum. The increase in lunar angular momentum causes the Moon to move farther away from the Earth at a rate of ~4 cm/a and to increase its orbital period. This increase in period has been determined accurately from LLR data.

Tidal Friction (4)

- The tidal bulge perturbs the orbit of a satellite, thus by ranging to satellites such as LAGEOS, the lag angle δ can be determined. The lunar torque on the Earth can also be determined from δ and thus the change in LOD can be calculated. This predicted increase in the LOD is about 25% larger than that implied by the historical eclipse record (~1.7 ms/century)
- The reason for this discrepancy is due to Postglacial Rebound, which cause a net transfer of mantle material toward the poles. This redistribution of internal mass decreases the earth's polar moment of inertia and give rise to the observed non-tidal acceleration of the Earth. Postglacial rebound also causes a net polar wander towards Hudson's Bay today

Tidal Friction (5)

- If the dissipation rate inferred from LLR and SLR are used to extrapolate the present lunar orbit backward in time, the Moon is predicted to be so close to the Earth 1.5 Ga ago that it would be torn apart by gravitational forces from the Earth. However, the Moon is over 4 Ga old. This implies that tidal friction is larger now than it was in the past. Since the dissipation is sensitive to the shape of the ocean basins and to the rotation rate, continental drift may be responsible for the temporal variation of tidal dissipation

Measurements of Non-tidal Acceleration

Source	$\dot{\omega}_3 / \Omega$ (10^{-10}/year)
Currot (1966)	0.7 + 0.3
Muller & Stephenson (1975)	1.5 + 0.3
Morrison (1973)	2.9 + 0.6
Lambeck (1977)	0.69 + 0.3

i.e. length of day decrease by ~0.7 ms/century

Wu & Peltier (1984) showed that Nontidal Acceleration
= the time rate of change of J_2 multiply by the constant $\frac{2M_E R_E^2}{3C}$

LAGEOS Measurements Of J_n dot

From Cheng et al (1997)

	$\dot{J}_n$ (x 10^{-11} /year)
n=2	-2.7 + 0.4
n=3	-1.3 + 0.5
n=4	-1.4 + 1.0
n=5	2.1 + 0.6
n=6	0.3 $\pm$0.7

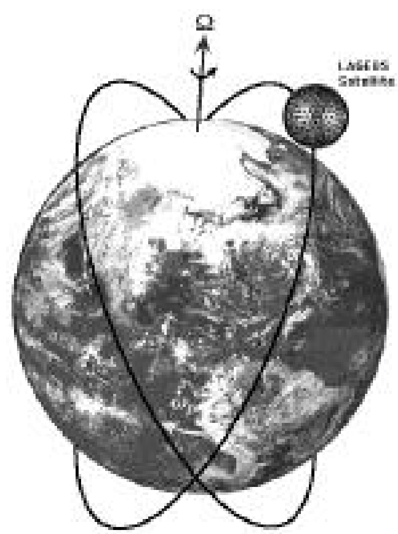

Rate of precession $\dot{\omega}_p = f(J_2, J_4, \ldots J_{2n})$

$$\Delta\phi = \frac{GM}{r} \sum_{n=2} \sum_{m=0}^{n} \left(\frac{a}{r}\right)^n J_{n,m} P_{n,m}(\cos\theta) \cos m(\lambda - \lambda')$$

Nontidal Acceleration

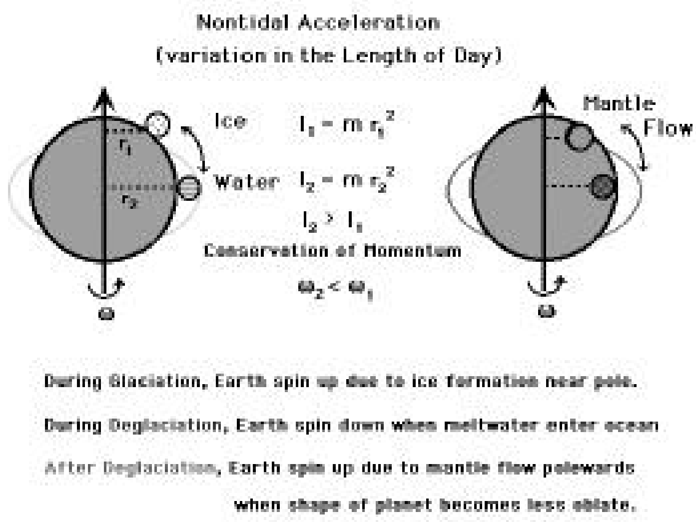

length of day decreases by ~0.7 ms/century

Secular Polar Wander

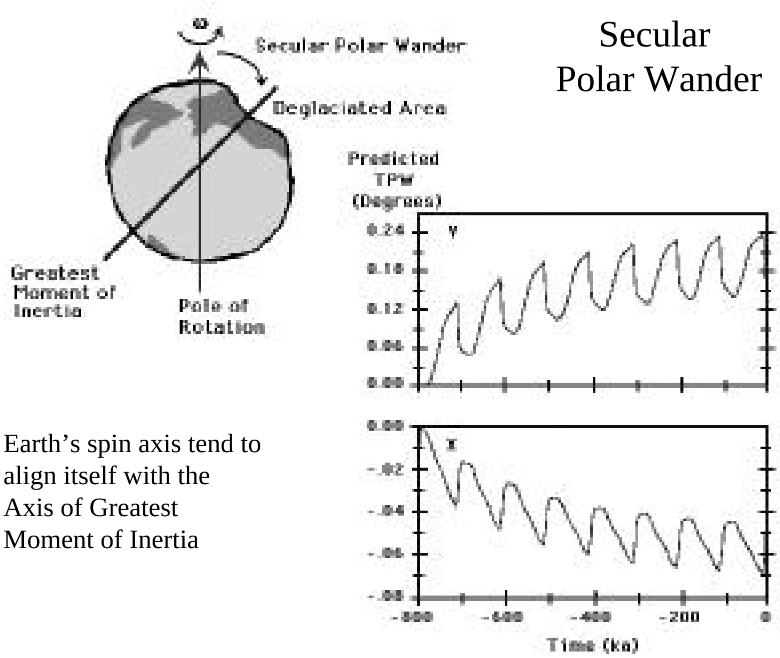

Earth's spin axis tend to align itself with the Axis of Greatest Moment of Inertia

Predicted True Polar Wander Path due to 8 Glacial Cycles

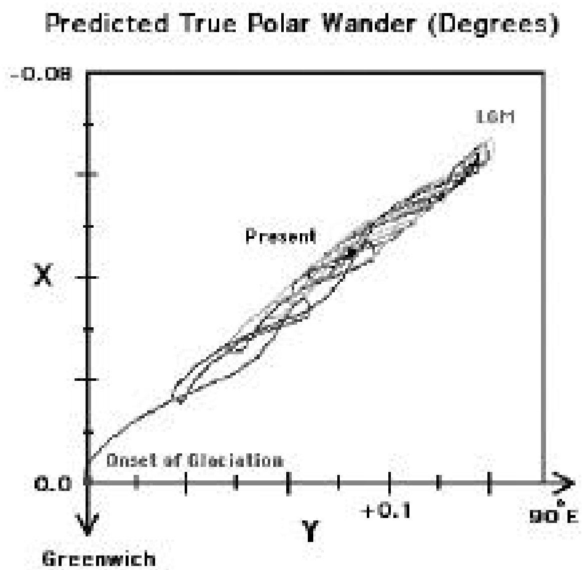

Euler Equation for the conservation of angular momentum:

$$\frac{d}{dt}\left(J_{ij}\omega_j\right) + \varepsilon_{ijk}\omega_j J_{kl}\omega_l = 0$$

In the unperturbed state, $\left[J_{ij}\right] = \begin{bmatrix} A & 0 & 0 \\ 0 & B & 0 \\ 0 & 0 & C \end{bmatrix}$ where $B \approx A$

with angular velocity vector : $\begin{bmatrix} 0 \\ 0 \\ \Omega \end{bmatrix}$

In the perturbed state, the angular velocity vector is $\begin{bmatrix} m_1 \\ m_2 \\ \Omega + m_3 \end{bmatrix}$

and $\left[J_{ij}\right] = \begin{bmatrix} A + I_{11} & I_{12} & I_{13} \\ I_{12} & A + I_{22} & I_{23} \\ I_{13} & I_{23} & C + I_{33} \end{bmatrix}$

Liouville's Equation- linearized Euler Equations

$$\frac{i}{\sigma_r}\dot{\boldsymbol{m}} + \boldsymbol{m} = \Psi \quad \text{and} \quad \dot{m}_3 = \dot{\psi}_3$$

where $\boldsymbol{m} = m_1 + i m_2$ and

$\sigma_r = \Omega \dfrac{(C-A)}{A}$ is the Chandler frequency of a rigid earth,

and the Excitation Functions are (Munk & MacDonald 1960):

$$\Psi = \psi_1 + i\psi_2 \qquad \psi_1 = \frac{I_{13}}{(C-A)} + \frac{\dot{I}_{23}}{\Omega(C-A)}$$

$$\psi_2 = \frac{I_{23}}{(C-A)} - \frac{\dot{I}_{13}}{\Omega(C-A)} \qquad \psi_3 = \frac{-I_{33}}{C}$$

$$\Psi = \Psi^{Rot} + \Psi^{Load}$$

First consider the Excitation due to Rotation:
following Lambeck(1980), the centrifugal potential is:

$$\chi = \tfrac{1}{3}\omega^2 r^2 + \frac{GM}{r}\left(\frac{a}{r}\right)^2 \sum_{m=0}^{2}\left[C_{2m}\cos(m\phi) + S_{2m}\sin(m\phi)\right] P_2^m(\cos\theta)$$

where $C_{20} = \dfrac{a^3}{6GM}\left(\omega_1^2 + \omega_2^2 - 2\omega_3^2\right) \quad k_2^T$

$$C_{21} = -\frac{a^3}{3GM}\omega_1\omega_3 \quad k_2^T \qquad C_{22} = \frac{a^3}{12GM}\left(\omega_2^2 - \omega_1^2\right) \quad k_2^T$$

$$S_{21} = -\frac{a^3}{3GM}\omega_2\omega_3 \quad k_2^T \qquad S_{22} = -\frac{a^3}{6GM}\omega_1\omega_2 \quad k_2^T$$

Using MacCullagh's formula (Munk & MacDonald 1960):

$$I_{13}^{Rot} \quad \frac{k_2^T}{k_f} \quad m_1 (C - A) \qquad\qquad I_{23}^{Rot} \quad \frac{k_2^T}{k_f} \quad m_2 (C - A)$$

where $$k_f = \frac{3G}{a^5 \Omega^2} (C - A)$$

Thus $$\psi_1^{Rot} = \frac{k_2^T}{k_f} \left(m_1 + \frac{\dot{m}_2}{\Omega} \right) \quad \frac{k_2^T}{k_f} \quad m_1$$

$$\psi_2^{Rot} = \frac{k_2^T}{k_f} \left(m_2 - \frac{\dot{m}_1}{\Omega} \right) \quad \frac{k_2^T}{k_f} \quad m_2$$

and $$\Psi^{Rot} = \psi_1^{Rot} + i\psi_2^{Rot} = \frac{k_2^T}{k_f} \left(m_1 + i m_2 \right)$$

Thus, Liouville's Equation becomes

$$\frac{i}{\sigma_r} \dot{\boldsymbol{m}} + \boldsymbol{m} - \frac{k_2^T}{k_f} \quad \boldsymbol{m} = \Psi^{Load}$$ Polar Motion

$$\dot{m}_3 = \dot{\psi}_3$$ Length of Day Variation

As shown in Wu & Peltier (1984), the first term in the equation for Polar Motion contains the contribution of the Chandler Wobble. Thus

$$\left[1 - k_2^T / k_f \right] \quad \boldsymbol{m} = \Psi^{Load}$$

where **m** only contains secular variations.

Surface Mass Load & Induced Deformation (1)

Inertia Perturbation for Deformable Earth is :

$$I_{ij} = \left[1 + k_2^L\right] \quad I_{ij}^R$$

where I_{ij}^R is the Inertia Perturbation for a Rigid Earth

Thus,

$$\psi_1^{Load} = \left(1 + k_2^L\right) \left(\frac{I_{13}^R}{(C-A)} + \frac{\dot{I}_{23}^R}{\Omega(C-A)} \right)$$

$$\psi_2^{Load} = \left(1 + k_2^L\right) \left(\frac{I_{23}^R}{(C-A)} - \frac{\dot{I}_{13}^R}{\Omega(C-A)} \right)$$

$$\psi_3^{Load} = -\left(1 + k_2^L\right) \frac{I_{33}^R}{C}$$

Surface Mass Load & Induced Deformation (2)

The Inertia Perturbation on a rigid earth :

$$I_{ij}^R = \int_a^{a+h} \iint_S \rho(\vec{x}) \left[x_r x_r \delta_{ij} - x_i x_j \right] dS dr$$

where S is the surface of the earth. Since $h<<a$,

$$I_{ij}^R = \iint_S \sigma(\theta, \phi, t) \left[x_r x_r \delta_{ij} - x_i x_j \right] dS$$

where

$$\sigma(\theta, \phi, t) = \sum_{n=0}^{\infty} \sum_{m=0}^{n} \left[\sigma_{nm1}(t) \cos(m\phi) + \sigma_{nm2}(t) \sin(m\phi) \right] P_n^m(\cos\theta)$$

Surface Mass Load & Induced Deformation (3)

Using the orthogonal relationship for un-normalized Associated Legendre function :

$$\iint \left[P_n^m(\cos\theta) \begin{matrix} \cos(m\phi) \\ \sin(m\phi) \end{matrix} \right]^2 dS = \frac{4\pi\,(n+m)!}{(2n+1)(n-m)!\,(2-\delta_{0m})}$$

Therefore:

$$I_{13}^R + iI_{23}^R = -\frac{4}{5}\pi a^4 \left[\sigma_{211} + i\sigma_{212}\right]$$

$$I_{33}^R = \frac{8}{3}\pi a^4 \left[\sigma_{001} - \frac{\sigma_{201}}{5}\right]$$

since mass is conserved in GIA $\sigma_{001} = 0$ therefore

$$I_{33}^R = -\frac{8}{15}\pi a^4 \sigma_{201}$$

Summary of Equations in Time Domain

$$\left[1 - k_2^T / k_f\right] \quad \left\{m_1 + i\ m_2\right\} = \psi_1^{Load} + i\psi_2^{Load}$$

$$\psi_1^{Load} = -\frac{4}{5}\pi a^4 \frac{\left(1 + k_2^L\right)}{(C - A)} \quad \left[\sigma_{211}(t) + \dot{\sigma}_{212}(t)/\Omega\right]$$

$$\psi_2^{Load} = -\frac{4}{5}\pi a^4 \frac{\left(1 + k_2^L\right)}{(C - A)} \quad \left[\sigma_{212}(t) - \dot{\sigma}_{211}(t)/\Omega\right]$$

$$\dot{m}_3 = \dot{\psi}_3^{Load}$$

$$\psi_3^{Load} = \frac{8}{15}\frac{\pi a^4}{C}\left(1 + k_2^L\right) \quad \sigma_{201}(t)$$

Variation in LOD and J_2-dot

$$\dot{m}_3(t) = \frac{8}{15}\frac{\pi a^4}{C}\frac{\partial}{\partial t}\left\{\left(1+k_2^L\right)\sigma_{201}(t)\right\}$$

Expanding the potential perturbation as surface mass density:

$$\phi(\theta,\psi,t) = ag\sum_{n=0}^{\infty}\sum_{m=0}^{n}\left[J_{nm1}(t)\cos(m\psi) + J_{nm2}(t)\sin(m\psi)\right]P_n^m(\cos\theta)$$

$$= \frac{4\pi a^3 g}{M}\sum_{n=0}^{\infty}\sum_{m=0}^{n}\left(\frac{1+k_n^L}{2n+1}\right)\left[\sigma_{nm1}(t)\cos(m\psi) + \sigma_{nm2}(t)\sin(m\psi)\right]P_n^m(\cos\theta)$$

Comparing the two :
$$J_{nmi}(t) = \frac{4\pi a^2}{M}\frac{\left[1+k_n^L(t)\right]}{(2n+1)}\sigma_{nmi}(t)$$

Therefore:
$$\boxed{\dot{J}_2(t) = -\frac{3C}{2a^2 M}\dot{m}_3(t)}$$

Love Number Approach for Polar Wander (1):

Load and Tidal Love Numbers

$$k_2^L(s) = k_2^{LE} + \sum_{i=1}^{N}\frac{r_i}{s-s_i} = -1 + l_s + s\sum_{i=1}^{N}\frac{r_i/s_i}{s-s_i}$$

$$k_2^T(s) = k_2^{TE} + \sum_{i=1}^{N}\frac{t_i}{s-s_i} = k_2^T(0) + s\sum_{i=1}^{N}\frac{t_i/s_i}{s-s_i}$$

defining
$$g_j = \frac{t_j/s_j}{\sum_{i=1}^{N}(t_i/s_i)} \qquad k_f = \frac{\sigma_r}{\sigma_o}\sum_{i=1}^{N}(t_i/s_i) \qquad \frac{\sigma_o}{\sigma_r} = \frac{k_2^T(0)-k_2^{TE}}{k_2^T(0)}$$

$$Q_{N-1}(s) = \left(\sum_{i=1}^{N}\frac{g_j}{s-s_i}\right)\prod_{j=1}^{N}(s-s_j) = \prod_{j=1}^{N-1}(s+\lambda_j)$$

$$q(s) = s\prod_{j=1}^{N-1}(s+\lambda_j) - \prod_{i=1}^{N}(s-s_i) \qquad R_j(s) = \prod_{j=1}^{N-1}(s+\lambda_j) - \prod_{i\neq j}(s-s_i)$$

Love Number Approach for Polar Wander (2):

$$\dot{m}_j(t) = \frac{\Omega}{A\sigma_o}\left[D_1 \dot{I}^R_{j3}(t) + D_2 I^R_{j3}(t) + \sum_{i=1}^{N-1} E_i \frac{\partial}{\partial t}\left\{ e^{-\lambda_i t} \quad I^R_{j3}(t) \right\} \right]$$

$$\left\langle m_j(t) \right\rangle = \frac{\Omega}{A\sigma_o}\left[D_1 I^R_{j3}(t) + D_2 \int_{t'=0}^{t} I^R_{j3}(t')\,dt' + \sum_{i=1}^{N-1} E_i \left\{ e^{-\lambda_i t} \quad I^R_{j3}(t) \right\} \right]$$

$$D_1 = l_s - \sum_{i=1}^{N} (r_i/s_i) = 1 + k_2^{LE}$$

$$D_2 = -l_s q(0) \Big/ \prod_{i=1}^{N-1} \lambda_i$$

$$E_i = \left[\frac{l_s q(-\lambda_i)}{\lambda_i} + \sum_{j=1}^{N} \frac{r_j R_j(-\lambda_i)}{s_j} \right] \Big/ \prod_{k \neq i}^{N-1} (\lambda_k - \lambda_i)$$

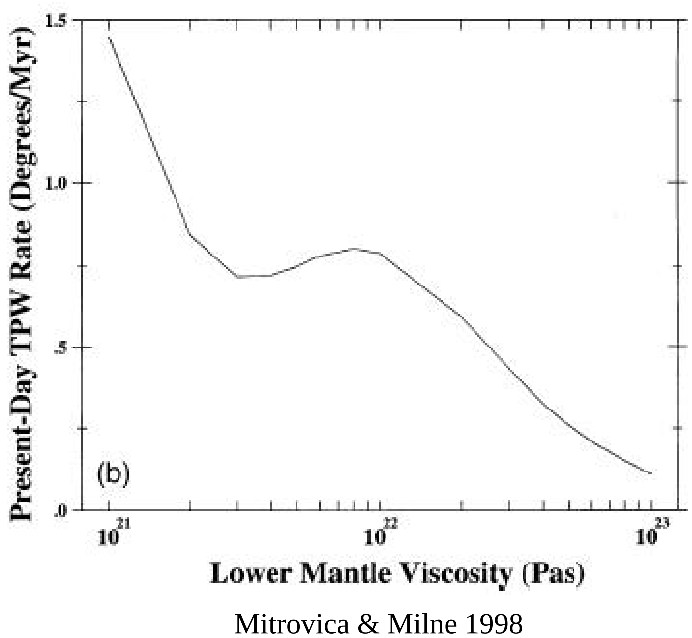

Mitrovica & Milne 1998

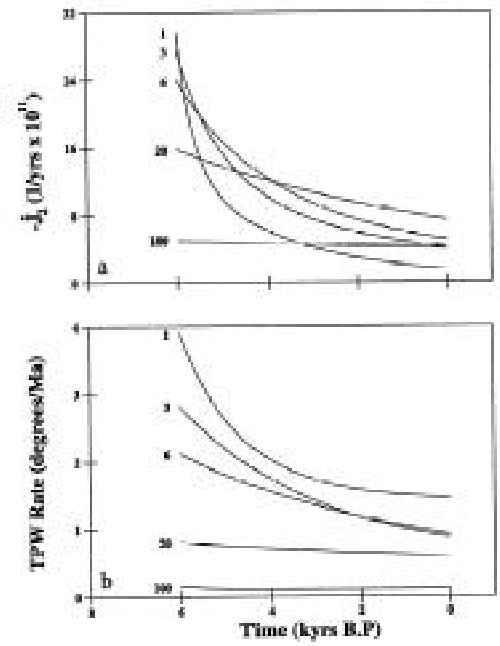

Mitrovica & Milne 1998

Sawtooth glacial cycles
Deglaciation ended at 6 ka BP
PREM Earth Models
100 km Lithosphere
1×10^{21} Pa-s Upper Mantle
$n \times 10^{21}$ Pa-s Lower Mantle

Polar Wander & J_2-dot

- Observation not all due to last deglaciation, current melting and other mantle processes (mantle convection, mountain building, etc.) may have contributions
- J_2-dot sensitive to lower mantle viscosity but not M1 mode nor lithospheric thickness
- Polar Wander Speed sensitive to :

  lower Mantle viscosity,

  lithospheric thickness

  compressibility

Some References

- O'Connell 1971, Geophys.J.R. Astron. Soc., 23:299-327
- Nakiboglu & Lambeck 1980, Geophys.J.R. Astron. Soc., 62:49-58
- Sabadini & Peltier 1981, Geophys.J.R. Astron. Soc., 66:553-578
- Sabadini, Yuen & Boschi 1982, JGR, 87:2885-2903
- Wu & Peltier 1984, Geophys.J.R. Astron. Soc., 76:753-791
- Yoder & Ivins 1985, EOS, 66:245
- Gasperini, Sabadini & Yuen 1986, GRL, 13:533-536
- Trupin, Meier & Wahr 1992, GJI, 108:1-5
- Spada, Sabadini, Yuen & Ricard 1992, GJI, 109:683-700
- Peltier & Jiang 1994, JGR, 101:3269-3290
- Vermeersen, Sabadini, Spada & Vlaar 1994, GJI, 117:610-624
- Vermeersen & Sabadini 1996, GJI, 126:735-761
- Mitrovica & Milne 1998, JGR 103:985-1005
- Johnston & Lambeck 1999, GJI, 136:537-558

Wu (1982)

Prove that the inertia perturbation due to deformation: $I_{ij}^{D} = k_2^{L} \quad I_{ij}^{R}$

By definition: $I_{ij}^{D} = \iiint\limits_V \rho_1 \left(x_r x_r \delta_{ij} - x_i x_j\right) dV + \iint\limits_S \rho_0(a)\left(a^2 \delta_{ij} - x_i x_j\right) u(a)\, dS$

Below, we will only consider I_{33}^{D} - the other components will follow similarly. For I_{33}^{D}, the above becomes: $I_{33}^{D} = \iiint\limits_V \rho_1 \left(x_1^2 + x_2^2\right) dV + \iint\limits_S \rho_0 \left(x_1^2 + x_2^2\right) u(a)\, dS$

The gravitational potential can be decomposed into the direct contribution from the load and internal mass redistribution: $\phi_1 = \phi_2 + \phi_3 = \sum\limits_n \left(1 + k_n\right) \Phi_{2,n} P_n^m(\cos\theta)$. So that $\nabla^2 \phi_2 = 0$ and $\nabla^2 \phi_3 = 4\pi G \rho_1$.

Now from Green's identity:

$$\iiint\limits_V \left(Z \nabla^2 Y - Y \nabla^2 Z\right) dV = \iint\limits_S \left(Z \hat{n} \cdot \vec{\nabla} Y - Y \hat{n} \cdot \vec{\nabla} Z\right) dS$$

using $Y = \phi_3$ and $Z = x_1^2 + x_2^2 = \frac{2}{3} r^2 \left[P_0^0(\cos\theta) - P_2^0(\cos\theta)\right]$

where $\nabla^2 Z = \frac{1}{r^2} \frac{\partial}{\partial r}\left(r^2 \frac{\partial Z}{\partial r}\right) + \frac{1}{r^2 \sin\theta} \frac{\partial}{\partial \theta}\left(\sin\theta \frac{\partial Z}{\partial \theta}\right) = 4$

$$\hat{n} \cdot \nabla Z = \frac{\partial}{\partial r} Z = \frac{4}{3} r \left[1 - P_2^0(\cos\theta)\right] = \frac{2}{r} Z$$

we get: $I_{33}^{D} = \frac{1}{4\pi G}\left[4 \iiint\limits_V \phi_3 dV + \frac{2}{3} a^2 \iint\limits_S \left(P_0^0 - P_2^0\right) \Gamma(a)\, dS\right]$

where $\Gamma = \frac{\partial}{\partial r}\phi_3 - \frac{2}{3}\phi_3 + 4\pi G \rho_0 u$

In the transformed s-domain, expanding: $\phi_3 = \sum\limits_n \Phi_{3,n}(r) P_n^0(\cos\theta)$, $u = \sum\limits_n U_n(r) P_n^0(\cos\theta)$,

$\Gamma = \sum\limits_n \Gamma_n(r) P_n^0(\cos\theta)$

then $\iiint\limits_V \phi_3 dV = 4\pi \int_0^a r^2 \Phi_{3,n}(r)\, dr$

and $\iint\limits_S \left(P_0^0 - P_2^0\right) \Gamma(a)\, dS = 4\pi a^2 \left[\Gamma_0(a) - \frac{1}{5}\Gamma_2(a)\right]$

thus, $I_{33}^{D} = \frac{4}{G} \int_0^a r^2 \Phi_{3,0}(r)\, dr + \frac{a^2 M}{g}\left[\frac{2}{3}\Gamma_0(a) - \frac{2}{15}\Gamma_2(a)\right]$

In order to express the Γ_n in terms of k_n^L use the definition of the gradient of potential:

$$Q_n = \frac{\partial}{\partial r}\Phi_{3,n} + \frac{(n+1)}{a}\Phi_{3,n} + 4\pi G\rho_0 U_n$$

and by comparing with the definition of Γ_n, we see that $\Gamma_n(a) = Q_n(a) - \frac{(n+3)}{a}\Phi_{3,n}(a)$

Since $Q_n(a) = 0$, $\Gamma_n(a) = -\frac{(n+3)}{a}\Phi_{3,n}(a) = (n+3)\frac{g}{M}k_n^L L_n$

where $L_n = a^2 \iint \sigma(\theta,\varphi) P_n^0(\cos\theta)\, dS = \frac{4\pi a^2}{(2n+1)}\sigma_{n01}$ and $I_{33}^R = -\frac{2}{3}a^2 L_2$

Thus, $I_{33}^D = \frac{4}{G}\int_0^a r^2 \Phi_{3,0}(r)\, dr + 2a^2 k_0^L L_0 - \frac{2}{3}a^2 k_2^L L_2$

For glacial loading events, the n=0 response is never excited because $\sigma_{001} = L_0 = 0$, thus in the transformed s-domain: $I_{33}^D = -\frac{2}{3}a^2 k_2^L L_2 = k_2^L I_{33}^R$

Other components can be derived similarly.

GIA with Nonlinear Rheology

- Definition
- Interaction between Ambient Tectonic Stress and 'Rebound' Stress (due to GIA process)
- Modeling with Tectonic-Rebound Stress Interaction
- Modeling without Tectonic-Rebound Stress Interaction

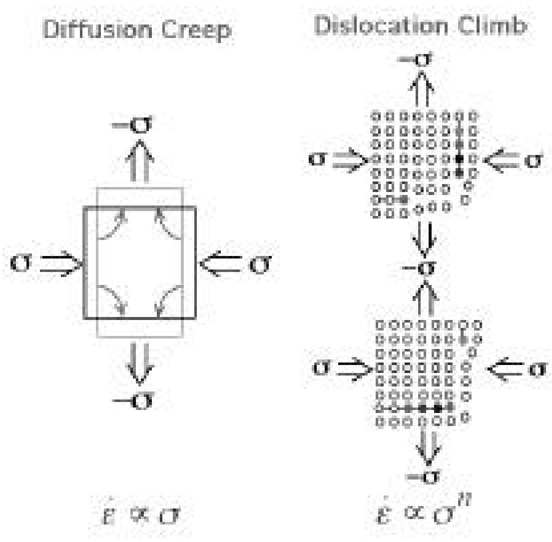

Diffusion creep dominates for low stress level or small grain size
Dislocation creep dominates for high stress level or large grain size

Steady State Creep Law: $\dot{\varepsilon} = A^* \sigma^n$

where $A^* = \frac{A}{\mu^n}\left(\frac{b}{d}\right)^m e^{-(E^* + PV^*)/RT}$

and $\mu \sim 80$ GPa, $b \sim 0.5$ nm

Effective Viscosity : $\eta \propto \sigma / \dot{\varepsilon}$

Flow law parameters for olivine

dislocation creep	dry	wet
A (/s)	3.5×10^{22}	2.0×10^{18}
n	3.5	3.0
m	0	0
E*	540	430
V*	15-25	10-20
diffusion creep		
A (/s)	8.7×10^{15}	5.3×10^{15}
n	1.0	1.0
m	2.5	2.5
E*	300	240
V*	6	5

Transition between Diffusion & Dislocation Creep

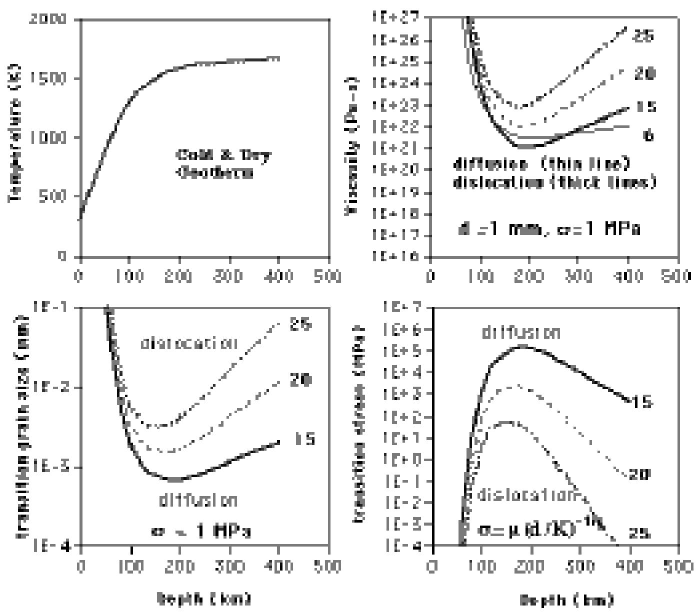

ViscoElastic Medium with Power Law:

$$\dot{\varepsilon}_{ij} = \dot{\varepsilon}^{E}_{ij} + \dot{\varepsilon}^{C}_{ij}$$

$$\dot{\varepsilon}^{C}_{ij} = A^{*}\, \sigma'^{\,n-1}_{E}\, \sigma'_{ij}$$

where $\sigma'_{E} = \sqrt{\frac{1}{2}\sigma'_{ij}\sigma'_{ij}}$

and $\sigma'_{ij} = \sigma_{ij} - \frac{1}{3}\sigma_{kk}\delta_{ij}$

Define : $\eta_{eff} = \dfrac{1}{3A^{*}\sigma'^{\,n-1}_{E}}$

GIA with Nonlinear Rheology

- Definition
- Interaction between Ambient Tectonic Stress and ‘Rebound’ Stress (due to GIA process)
- Modeling with Tectonic-Rebound Stress Interaction
- Modeling without Tectonic-Rebound Stress Interaction

Tectonic & Rebound Stress Interaction 1

If both rebound & tectonic stresses are present

$$\sigma'_{ij} = \sigma'^{T}_{ij} + \sigma'^{R}_{ij}$$

Substituting this into the creep law $\dot{\varepsilon}^{C}_{ij} = A^{*}\, \sigma'^{\,n-1}_{E}\, \sigma'_{ij}$

where $\sigma'_{E} = \sqrt{\frac{1}{2}\, \sigma'_{ij}\, \sigma'_{ij}}$

gives $\sigma'_{E} = \sigma'_{TE} + \frac{1}{2}\, \frac{\sum_{i,j}\left(\sigma'^{T}_{ij}\, \sigma'^{R}_{ij}\right)}{\sigma'_{TE}}$

$$\dot{\varepsilon}^{C}_{ij} = \dot{\varepsilon}^{T}_{ij} + A\, \sigma'^{\,n-1}_{TE}\, \sigma'^{R}_{ij} + A^{*}\, \frac{(n-1)}{2}\, \sigma'^{\,n-3}_{TE}\, \sigma'^{T}_{ij} \left(\sum_{i,j}\left[\sigma'^{T}_{ij}\, \sigma'^{R}_{ij}\right]\right)$$

where $\dot{\varepsilon}^{T}_{ij} = A^{*}\, \sigma'^{\,n-1}_{TE}\, \sigma'^{T}_{ij}$ $\qquad \sigma'_{TE} = \sqrt{\frac{1}{2}\left(\sum_{i,j} \sigma'^{T}_{ij}\, \sigma'^{T}_{ij}\right)}$

Tectonic & Rebound Stress Interaction 2

Thus, the strain rate seen by rebound is:

$$\dot{\varepsilon}^{R}_{ij} = A^{*}\, \sigma'^{\,n-1}_{TE}\, \sigma'^{R}_{ij} + A^{*}\, \frac{(n-1)}{2}\, \sigma'^{\,n-3}_{TE}\, \sigma'^{T}_{ij} \left(\sum_{i,j} \sigma'^{T}_{ij}\, \sigma'^{R}_{ij}\right)$$

From $\qquad \eta_{eff} = \frac{1}{3\, A^{*}\, \sigma'^{\,(n-1)}_{E}}$

one gets $\qquad \eta_{eff} = \frac{\eta^{T}_{eff}}{1 + (n-1)\left(\frac{1}{2}\, \frac{\sum_{i,j}\left[\sigma'^{T}_{ij}\, \sigma'^{R}_{ij}\right]}{\sigma'^{\,2}_{TE}}\right)}$

where $\qquad \eta^{T}_{eff} = \frac{1}{3\, A^{*}\, \sigma'^{\,n-}_{TE}}$

Tectonic & Rebound Stress Interaction 3

Consider the case when rebound & tectonic stress are orthogonal

$$\sum_{i,j} \sigma'^{T}_{ij}\, \sigma'^{R}_{ij} = \sigma'^{T}_{kl}\, \sigma'^{R}_{kl}$$

then

$$\dot{\varepsilon}^{R}_{kl} = \frac{1}{2} A^* \sigma'^{\,n-1}_{TE} \left[(n-1)\, \sigma'^{T\,2}_{kl}\, \sigma'^{\,2}_{TE} + 2 \right] \sigma'^{R}_{kl}$$

$$\dot{\varepsilon}^{R}_{ij} = A^* \sigma'^{\,n-1}_{TE}\, \sigma'^{R}_{ij}$$

Thus, although the creep law is nonlinear, rebound only ‘sees’ a linear creep law with the effective viscosity dependent on the tectonic stress distribution.

Also, the creep law seen by the ij-th component is different from the kl-component - thus rebound sees a linear but anisotropic creep law.

Question:

Can observations of postglacial rebound tell whether the rheology of the mantle is linear or nonlinear?

Answer:

Yes for RSL sites outside the ice margin !

The tectonic stress level is important too!

Interaction of Ambient Stress with Rebound Stress

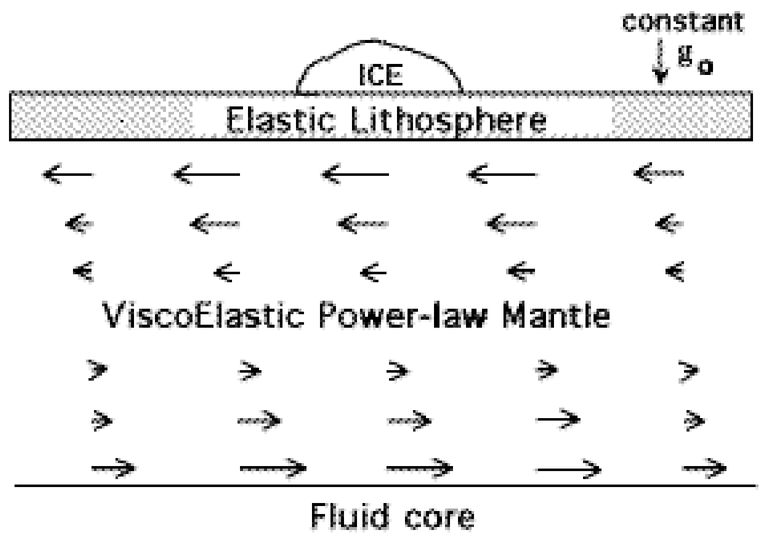

Find the combination in
(A*, Tectonic Stress Level)
that can fit the sealevel data in Laurentia

Location of Relative Sea level Sites with lengthy records

13 sites inside former ice margin
4 sites at the former ice margin
14 sites outside former ice margin

Total of 31 sites with lengthy records

Uniform Nonlinear Rheology A=3E-36 n=3

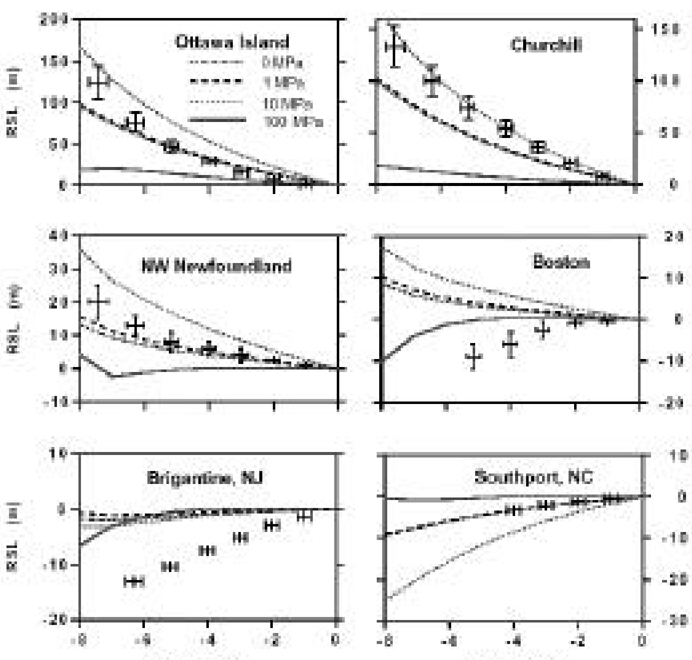

Uniform Nonlinear Rheology A=3E-35 n=3

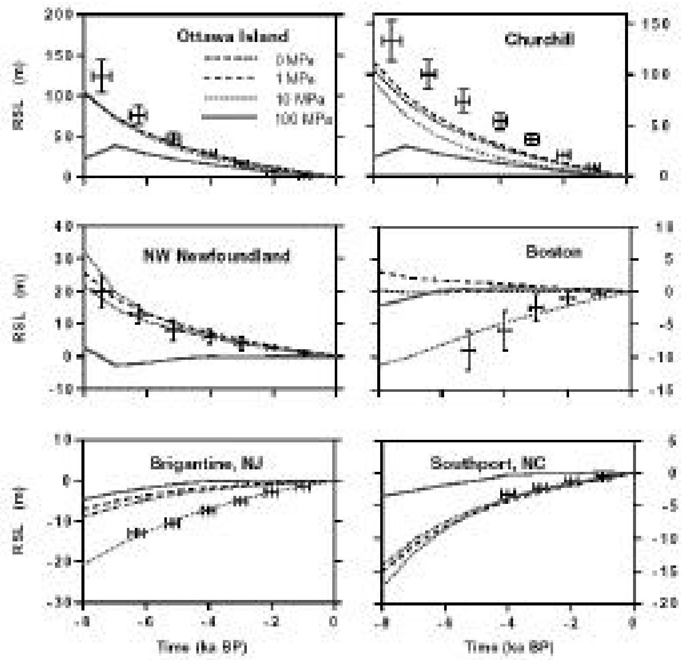

Uniform Nonlinear Rheology A=3E-34 n=3

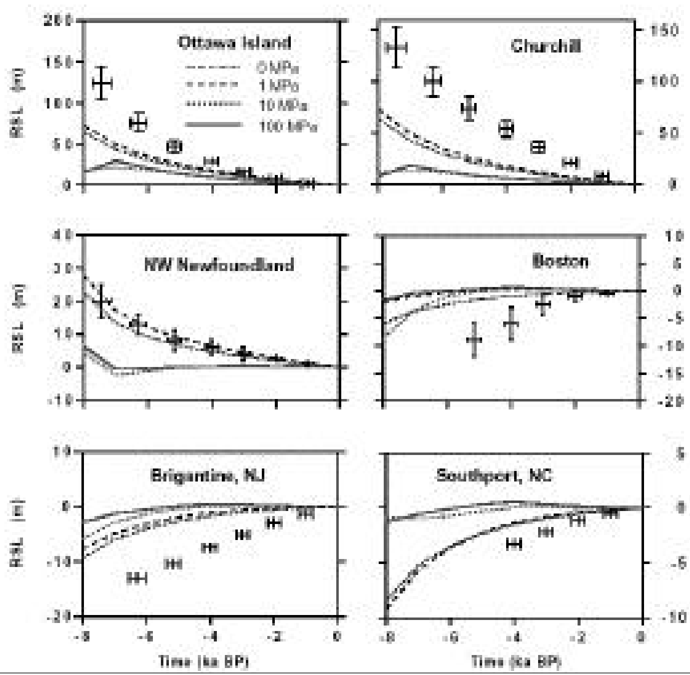

Summary for the case with Tectonic-Rebound Stress Interaction:

- RSL data just outside the ice margin can distinguish linear mantle from nonlinear mantle
- RSL data inside the ice margin can be explained by both linear and nonlinear rheology
- Nonlinear Uniform Mantles with $A=3x10^{-35}$, n=3 and Tectonic Stress Level ~ 10 MPa can explain the RSL data in and around Laurentia

Karato (1998): Since the strain due to GIA is orders of magnitude smaller than tectonic strain, there is no interaction between rebound & tectonic stress

Rheology Models considered

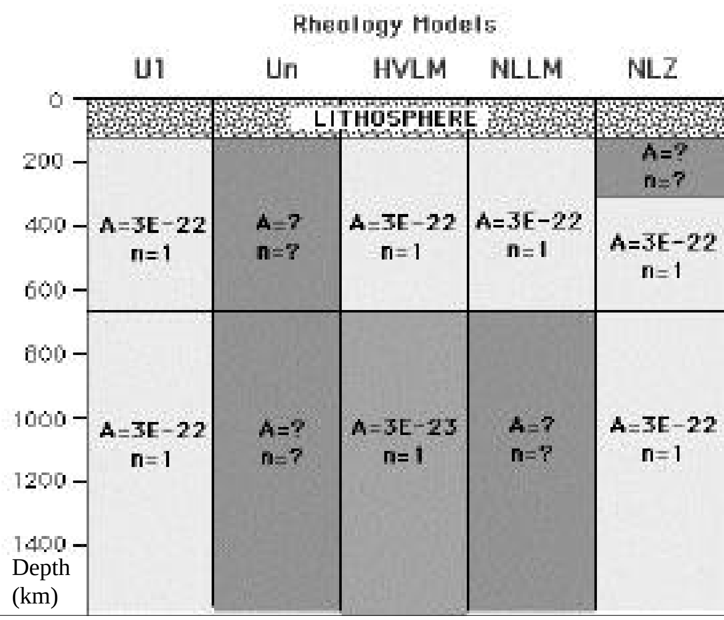

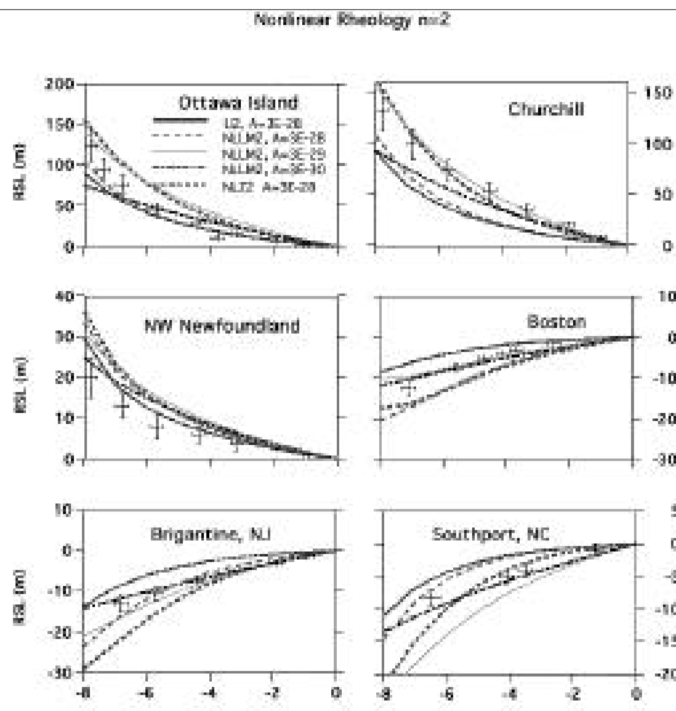

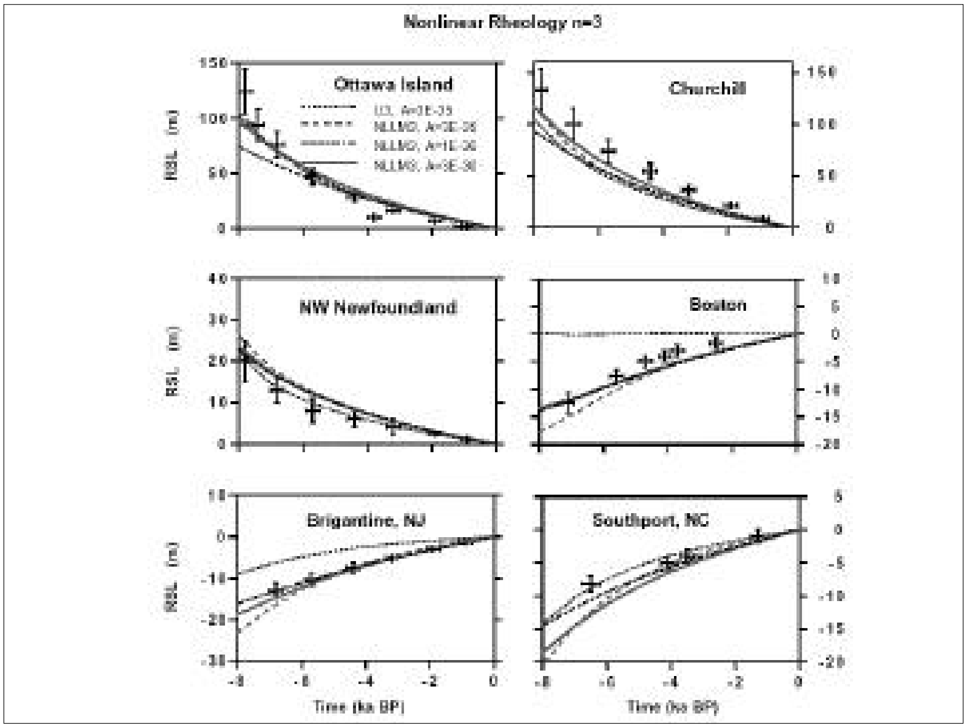
Nonlinear Rheology n=3
Ottawa Island
Churchill
NW Newfoundland
Boston
Brigantine, NJ
Southport, NC
RSL (m)
Time (ka BP)

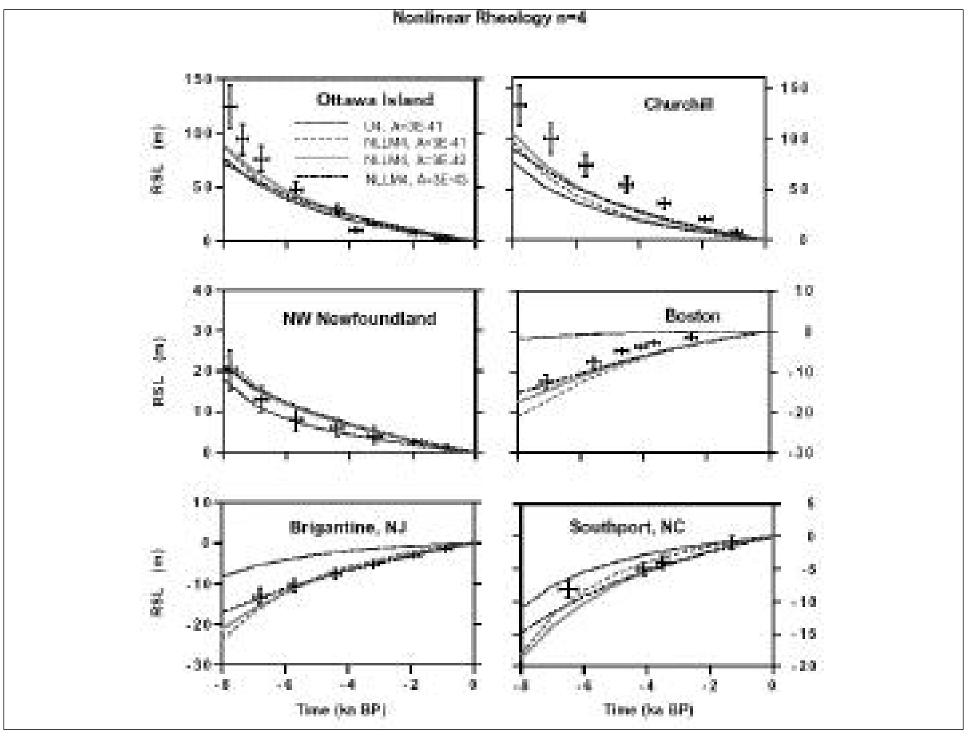
Nonlinear Rheology n=4
Ottawa Island
Churchill
NW Newfoundland
Boston
Brigantine, NJ
Southport, NC
RSL (m)
Time (ka BP)

For Uniform Mantles with Nonlinear Rheology, increasing the ICE3G thickness by a factor of h do NOT help with explaining the RSL data outside the ice margin

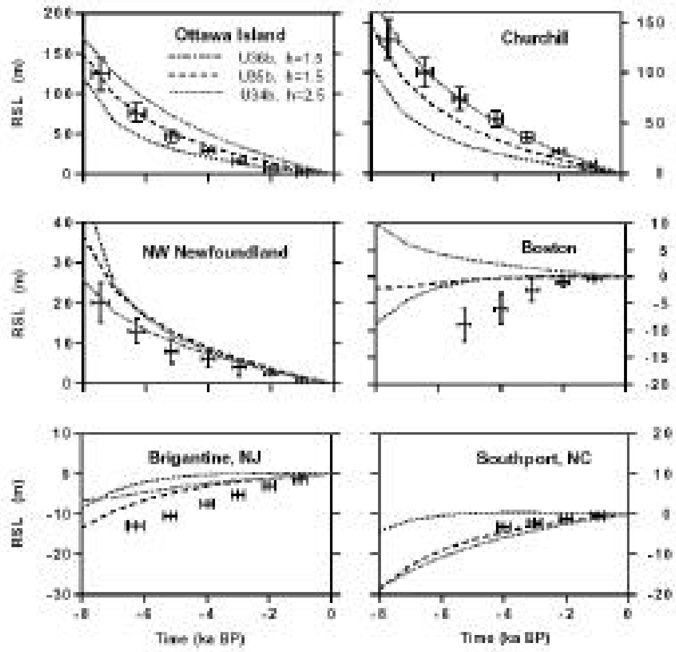

$$\chi^2 = \frac{1}{M}\sum_{n=1}^{M}\left(\frac{\zeta_{observed} - \zeta_{predicted}}{s}\right)^2$$

ζ = sealevel height

s = standard deviation of error in height

M = number of sealevel observations

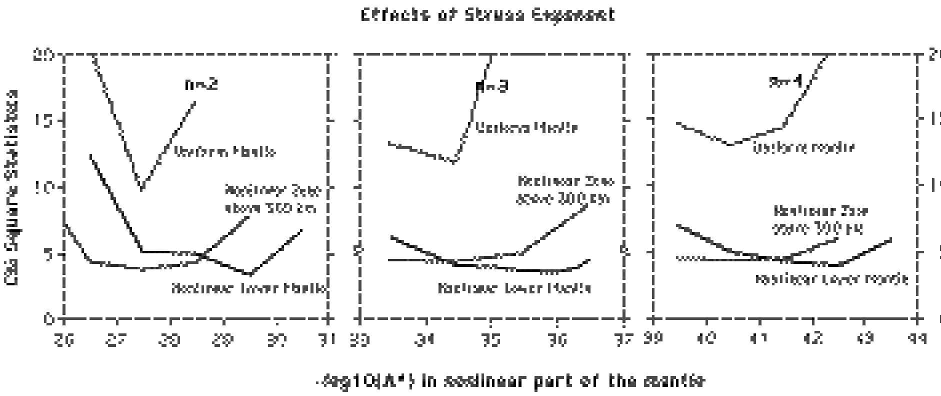

Comparing Predictions with Observations

- Relative sea levels
- Uplift Rate
- Horizontal velocity
- Rate of change of Absolute Gravity
- J2-dot (2nd degree harmonic of the Earth’s gravity field)

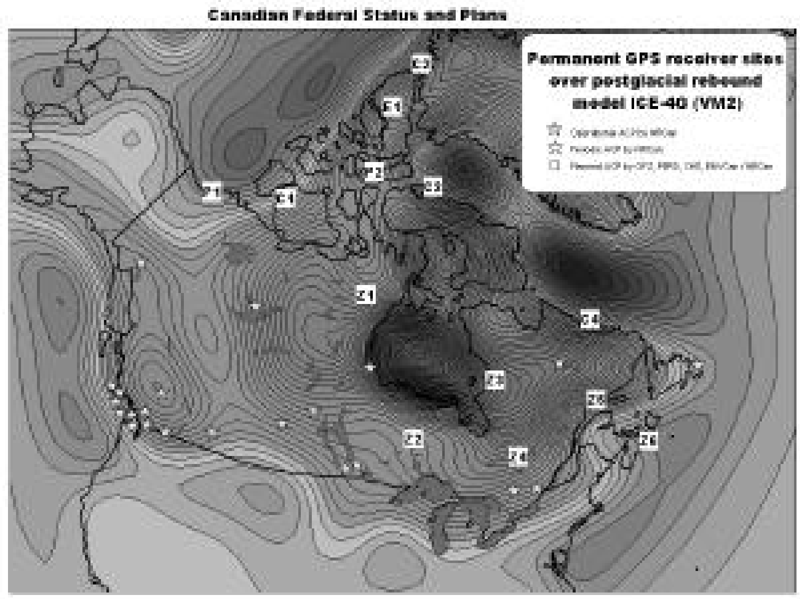

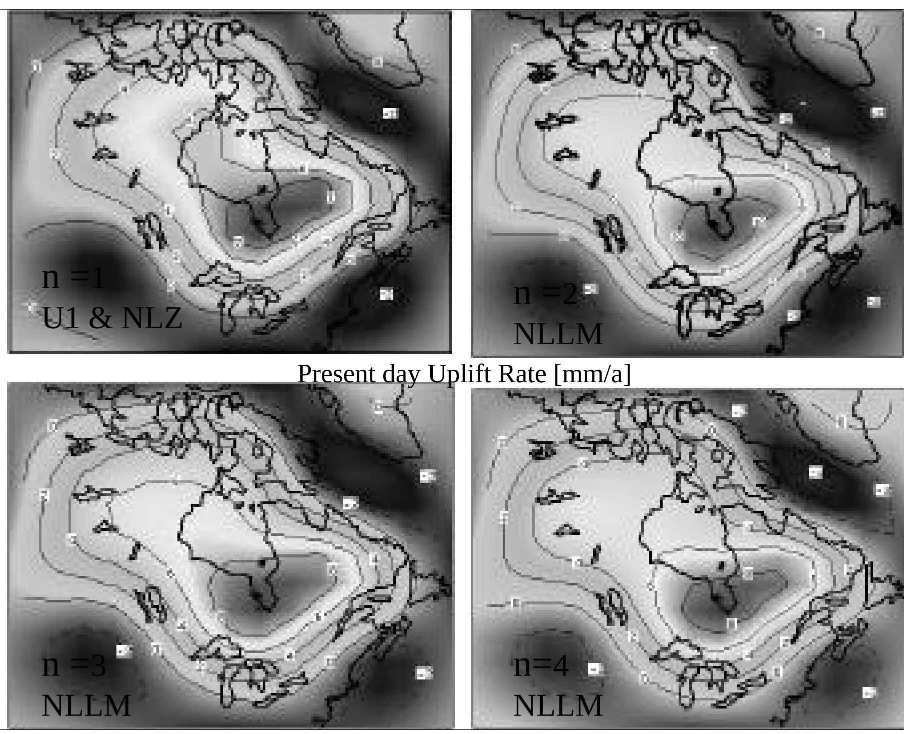

Present day Uplift Rate [mm/a]

Present day Uplift Rate [mm/a]
Tectonic Stress Level= 10 MPa , A=3E-35 n=3

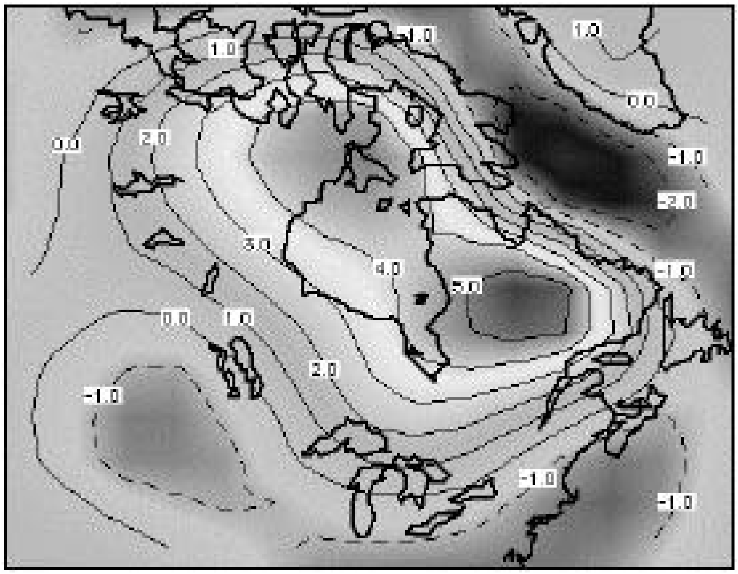

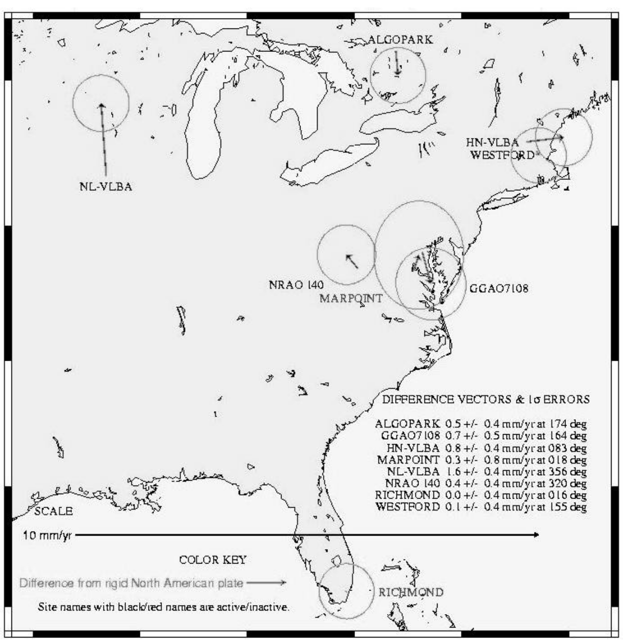

Goddard Space Flight Center VLBI Solution KB 2001cn Version 1

Difference from Rigid North American Plate Velocity NUVEL1A-NNR

1 σ (realistic) Error ellipses

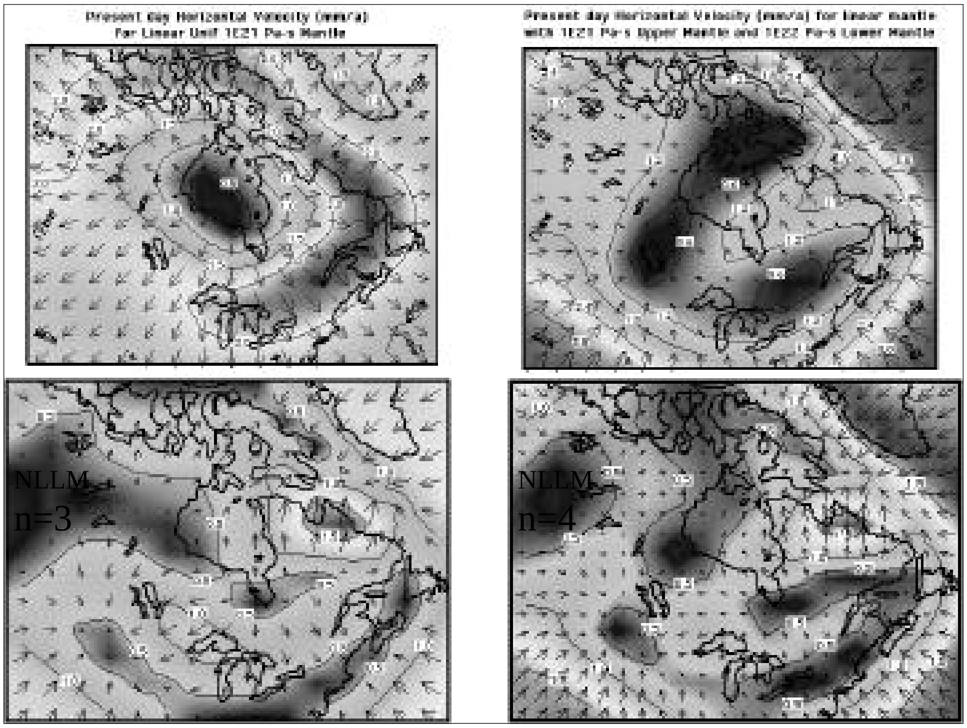

Horizontal Velocity [mm/a]
Tectonic Stress Level= 10 MPa , A=3E-35 n=3

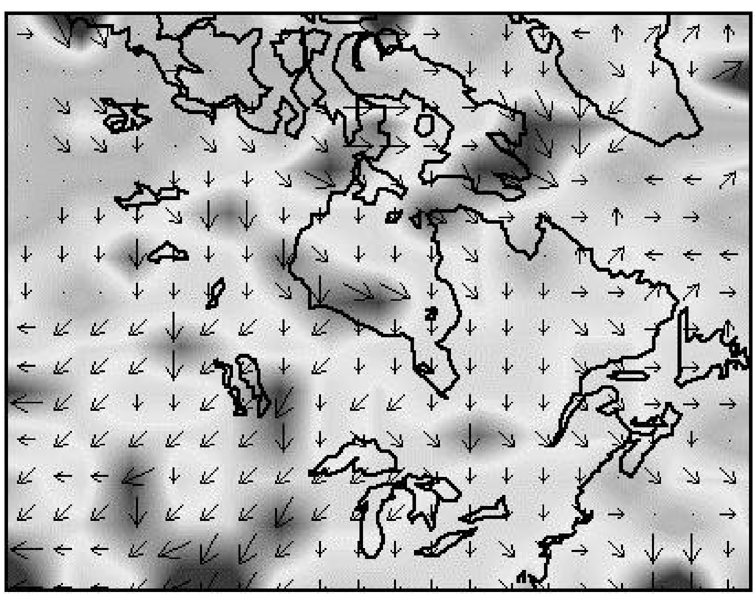

Comparing Predictions with Observations

- Relative sea levels
- Uplift Rate
- Horizontal velocity
- Rate of change of Absolute Gravity
- J2-dot (2nd degree harmonic of the Earth's gravity field)

Absolute Gravimeter FG5 & measured Rates of Change in Gravity

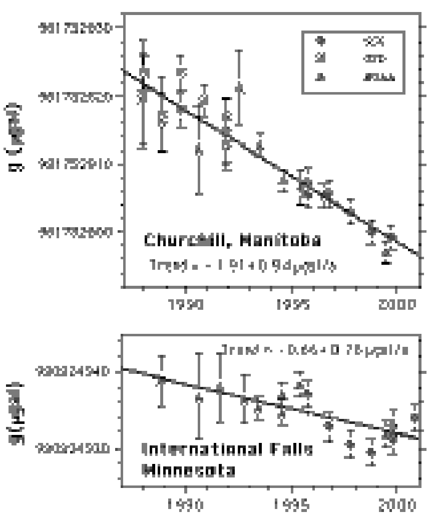

(Courtsey of A. Lambert)

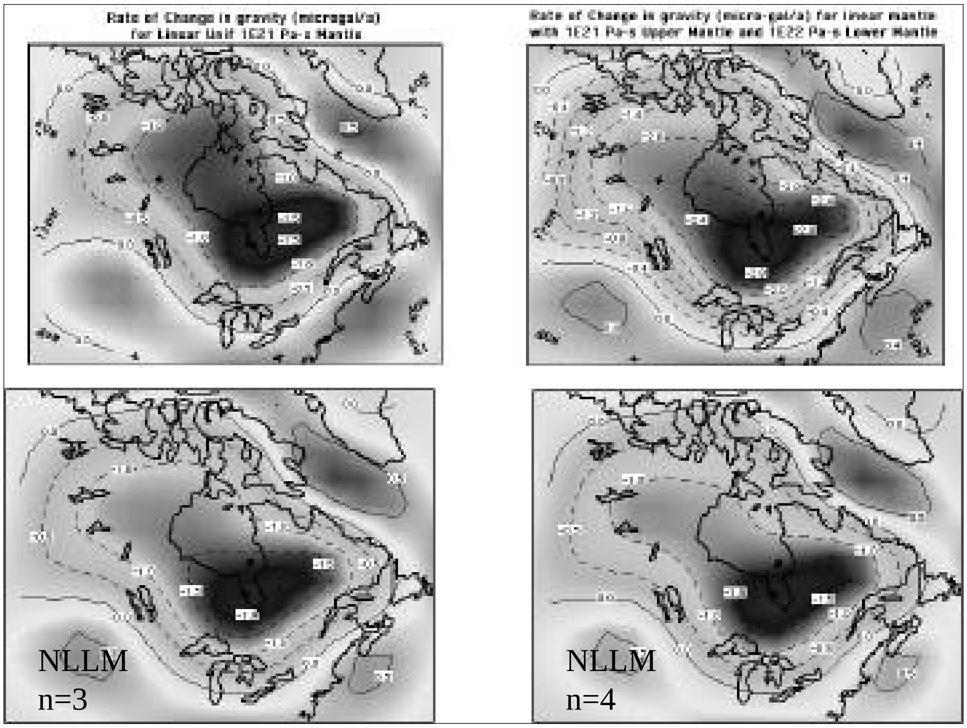

Gravity Rate of Change (μgal/a)
Tectonic Stress Level= 10 MPa , A=3E-35 n=3

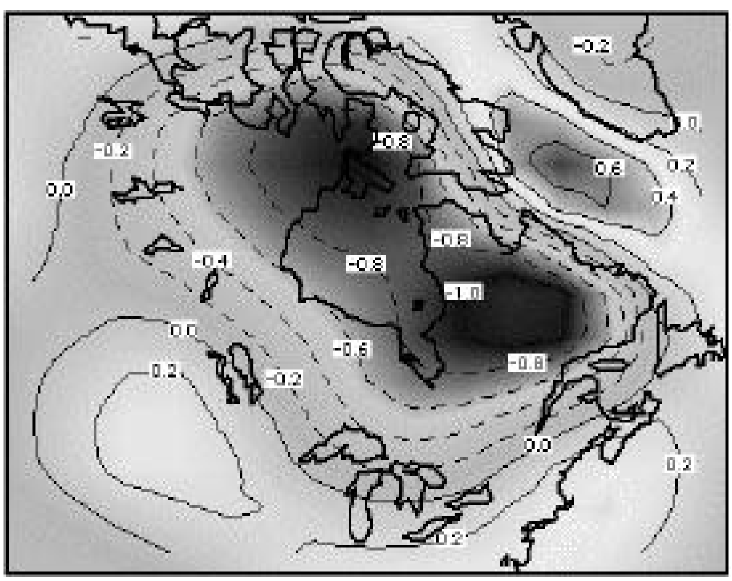

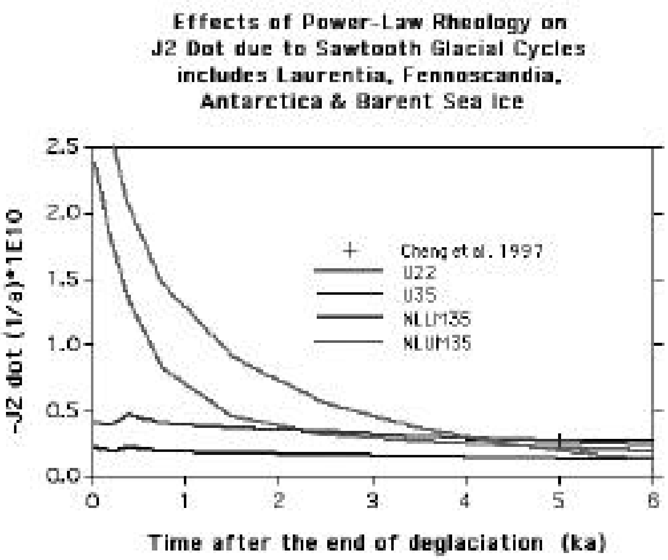

Summary

- Relative sea levels:

  1) reject uniform mantle with nonlinear rheology unless there is rebound-tectonic stress interaction and tectonic stress level is ~ 10 MPa and $A^* = 3\text{x}10^{-35}$ n=3

  2) Nonlinear Lower Mantle has the best Chi-Square fit

  3) Thin nonlinear zone below the lithosphere also acceptable
- Uplift Rate: future constraint
- Horizontal velocity: NLLM preferred?
- Rate of change of Absolute Gravity:NLLM acceptable
- J2-dot: NLLM acceptable

Future Work

- For Surface Motion & Gravity, include:
  a) Spherical Self-Gravitating Earth
  b) Self-Gravitating sealevels
  c) Compressibility
- For J2-dot , include :
  a) Self-Gravitating sealevels
  b) Compressibility
  c) Recent melting events

END